Lava-ground ice interactions in Elysium Planitia, Mars: Geomorphological and geospatial analysis of the Tartarus Colles cone groups

Lava–ground ice interactions in Elysium Planitia, Mars: Geomorphological and geospatial analysis of the Tartarus Colles cone groups

Christopher W. Hamilton,[1] Sarah A. Fagents,[1] and Thorvaldur Thordarson[2]

Received 21 May 2010; revised 2 November 2010; accepted 8 November 2010; published 5 March 2011.

[1] The western Tartarus Colles cone groups are located on Mars between northeastern Elysium Planitia and southern Arcadia Planitia (25°N–27°N and 170°E–171°E). This region contains >40,000 cratered cones covering a total area >2000 km^2. These landforms have been interpreted as volcanic rootless constructs (VRCs) that were produced by explosive lava-water interactions ~75–250 Ma ago. To better constrain their paleoenvironmental significance, we develop photogeological maps, morphological descriptions, lava thickness estimates, and statistical nearest neighbor (NN) analyses. The VRC-hosting Tartarus Colles lava flow exhibits bimodal thicknesses of 25–30 m and 55–60 m, whereas lava thickness associated with rootless eruption sites are unimodal, with a mean of 58 ± 8 m at 1 standard deviation (σ). Rootless eruption sites occur in 36 continuous domains with >10 rootless eruption sites per square kilometer and population sizes (N) >30. Renormalized Poisson NN analyses show that rootless eruption sites in 26 of 31 domains with $N < 3000$ are randomly distributed within 2σ confidence limits, whereas four of five domains with $N > 3000$ exhibit statistically significant clustering beyond 2σ. Regional clustering of rootless eruption sites in ~60 m thick lava is interpreted to be the result of a minimum lava thickness threshold required to volatilize ground ice and generate rootless eruptions before the lava core solidifies. Ground ice continued to melt after VRC formation and formed pitted terrains through thermokarstification. Widespread VRCs and pitted terrains in the Tartarus Colles region imply the presence of a major fossil hydrothermal system that was generated by lava–ground ice interactions during the late to middle Amazonian.

Citation: Hamilton, C. W., S. A. Fagents, and T. Thordarson (2011), Lava–ground ice interactions in Elysium Planitia, Mars: Geomorphological and geospatial analysis of the Tartarus Colles cone groups, *J. Geophys. Res.*, *116*, E03004, doi:10.1029/2010JE003657.

1. Introduction

[2] Rootless eruptions involve explosive interactions between lava and external water [*Thorarinsson*, 1951, 1953] and can include two end-member heat transfer mechanisms [*Fagents and Thordarson*, 2007]: "Static" conduction of heat through a stable basal lava crust to an underlying volatile-bearing substrate, or "dynamic" heat transfer involving physical mixing of lava and external water. *Fagents and Thordarson* [2007] demonstrate that dynamic heat transfer mechanisms are more common, but in either case, when the gas pressure beneath the lava flow exceeds the lithostatic pressure of the overburden and its mechanical strength, lava and substrate will be excavated from a rootless eruption site and deposited onto surrounding surfaces. The resulting landforms have been variously termed "rootless cones," "hydrovolcanic cones," "phreatovolcanic cones," and "pseudocraters." However, we favor the term volcanic rootless construct (VRC) because of its broader morphological scope, which encompasses morphologies that lack clearly expressed conical structures and/or craters, and because the term has less specific genetic implications, thereby admitting the possibility that rootless eruptions on some planetary bodies may be driven by volatile sources other than groundwater.

[3] VRCs commonly exhibit crater-in-cone morphologies and occur in groups with populations ranging from tens to tens of thousands. On Earth, VRCs are typically 2–450 m in basal diameter, 1–35 m in height, and form groups covering areas of up to ~150 km^2 [*Fagents and Thordarson*, 2007]. On Mars, VRC analogs are generally larger, with basal diameters of 30–1000 m, heights of >25 m [*Fagents et al.*, 2002], and domain areas covering >1000 km^2 [*Hamilton et al.*, 2010c].

[4] On Mars, cone groups in Elysium Planitia have a controversial origin, with researchers favoring either volcanic or periglacial formation mechanisms. Those favoring a volcanic origin claim that the cones groups in Elysium Planitia were formed by rootless eruptions [e.g., *Allen*, 1979; *Hartmann and Berman*, 2000; *Lanagan et al.*, 2001; *Greeley and Fagents*,

[1]Hawaii Institute of Geophysics and Planetology, University of Hawai'i, Honolulu, Hawaii, USA.
[2]School of Geosciences, University of Edinburgh, Edinburgh, U. K.

0148-0227/11/2010JE003657

2001; *Fagents et al.*, 2002; *Fuller and Head*, 2002; *Plescia*, 2003; *Bruno et al.*, 2004, 2006; *Baloga et al.*, 2007; *Fagents and Thordarson*, 2007; *Jaeger et al.*, 2007, 2008, 2010; *Keszthelyi et al.*, 2008, 2010; *Lanz and Saric*, 2009; *Hamilton et al.*, 2010b, 2010c]. In contrast, proponents of a nonvolcanic origin claim that the cones are ice-cored mounds (i.e., pingos) in varying states of preservation that formed through periglacial processes [e.g., *Burr et al.*, 2005; *Page and Murray*, 2006; *Page*, 2007, 2008; *Page et al.*, 2009]. These interpretations have vastly different paleoenvironmental implications and have even prompted *Page et al.* [2009] to call for a critical reexamination of the geology of the Elysium region and the paradigm of young "plains-forming" volcanism on Mars. Nevertheless, with new data provided by the High Resolution Imaging Science Experiment (HiRISE) camera on board the Mars Reconnaissance Orbiter (MRO), there is an emerging consensus that cone groups in Athabasca Valles and Cerberus Palus were misinterpreted as pingos and that these landforms are instead the products of explosive lava-water interactions [*Bruno et al.*, 2006; *Jaeger et al.*, 2007, 2008, 2010; *Keszthelyi et al.*, 2010; *Burr et al.*, 2009a, 2009b; *Dundas and McEwen*, 2010].

[5] In this study, we provide a historical overview of the investigation of Martian cone groups and present insights into the architecture of VRC groups on Earth and Mars. We then compare the morphological and geospatial characteristics of conical landforms in the western Tartarus Colles region of Mars to VRCs in Iceland. These analyses provide new evidence to support the interpretation that the Tartarus Colles cone groups are the products of explosive lava-water interactions. This information is important because of the widespread distribution of ground ice in the Martian regolith [*Squyres et al.*, 1992; *Mellon and Jakosky*, 1995], which could have been heated by volcanic sources to generate hydrothermal systems. Such fossil hydrothermal systems are significant because they could have provided habitable environments for life on Mars by providing liquid water and energy, which could sustain the metabolic functions of some biological organisms [*Squyres et al.*, 1987; *Shock*, 1997; *Jakosky and Shock*, 1998; *Link et al.*, 2005]. The study of explosive lava-water interactions can thus help to locate possible sites of fossil hydrothermal systems, infer paleoclimate conditions, explore volcanic processes, and identify water resources that could potentially be used by future robotic and human missions to Mars. These themes address many of the highest-priority goals within the current era of Mars research [*Mars Exploration Program Analysis Group (MEPAG)*, 2008], which include determining whether life ever arose on Mars, understanding Martian climate history and processes, characterizing the evolution of the Martian surface and interior, and preparing for human exploration.

2. Background Information

2.1. Historical Overview of the Study of Martian Cone Groups

[6] During the 1970s, cameras on board Mariner 9, Viking Orbiter 1, and Viking Orbiter 2 provided abundant evidence for widespread paleovolcanism on Mars [*Allen*, 1979; *Greeley and Spudis*, 1981]. Within some volcanic regions, kilometer-scale cones, domes, knobs, and mounds were identified in 30–300 m/pixel Viking Orbiter imagery and interpreted as analogs to Icelandic rootless cones [*Greeley and Theilig*, 1978; *Lucchitta*, 1978, 1981; *Allen*, 1979; *Frey et al.*, 1979, 1981; *Frey and Jarosewich*, 1982; *Mouginis-Mark*, 1985]. However, based on higher-resolution data, the identities of many of these landforms appear to have been misinterpreted, which has led to a consensus that the Martian cratered cone groups include a diverse range of landforms [*Farrand et al.*, 2005; *Jaeger et al.*, 2007; *Burr et al.*, 2009a; *Dundas and McEwen*, 2010].

[7] In the 1990s, the Mars Observer Camera (MOC) [*Malin et al.*, 1992], on board the Mars Global Surveyor (MGS), started to acquire images at much higher spatial resolutions (1.5–10 m/pixel) and revealed features that were clearly more similar to terrestrial rootless cones in terms of their size, morphology, and lava flow associations [*Lanagan et al.*, 2001]. *Lanagan et al.* [2001], *Greeley and Fagents* [2001], and *Fagents et al.* [2002] also used MOC images to compare Martian cone groups in Cerberus Palus, Marte Vallis, and Amazonis Planitia to the largest VRCs in Iceland, and determined that both sets of geologic features have similar morphologies and planimetric dimensions. These observations strengthened the hypothesis that these cratered cone groups formed by rootless eruptions; however, alternative processes, such as mud volcanism [*Farrand et al.*, 2005] and pingo formation [*Burr et al.*, 2005; *Page and Murray*, 2006; *Page*, 2007, 2008; *Page et al.*, 2009] have also been proposed for some cone groups on Mars.

2.2. The Paleoenvironmental Significance of Martian VRCs

[8] Before the discovery of VRC analogs on Mars, it was widely believed that the Martian near-surface environment would be desiccated at middle to low latitudes because of the instability of ground ice in these regions under current Martian climate conditions [*Clifford and Hillel*, 1983; *Fanale et al.*, 1986]. However, if Martian cone groups and terrestrial VRCs share a common formation mechanism (namely, explosive lava-water interaction), then the presence of low-latitude VRCs within young lava flows on Mars implies that near-equatorial groundwater (or ice) must have been present within the past 10 Ma [*Lanagan et al.*, 2001]. VRCs are therefore useful paleoenvironmental indicators that can provide information about both volcanic processes and near-surface volatile stability [*Greeley and Fagents*, 2001; *Fagents et al.*, 2002; *Head and Wilson*, 2002; *Fagents and Thordarson*, 2007; *Jaeger et al.*, 2007, 2008, 2010]. Nevertheless, uncertainty remains regarding the origin of the volatiles [*Keszthelyi et al.*, 2010]. For instance, Martian rootless eruptions could have involved H_2O from ephemeral sources, such as massive aqueous floods from Cerberus Fossae [*Head and Wilson*, 2002; *Head et al.*, 2003; *Plescia*, 2003] and/or the groundwater could have been atmospherically derived in response to obliquity-driven climate change [*Keszthelyi et al.*, 2010; *Hamilton et al.*, 2010c]. Associations between putative aqueous flood deposits and VRCs in Marte Vallis [*Lanagan et al.*, 2001; *Fuller and Head*, 2002] suggest that explosive lava-water interactions in this region of Mars involved surface and/or near-surface water that was released during syneruptive flooding events. However, at other localities, such as the Tartarus Colles region, VRC-hosting lava flows appear to overlie other lava flows rather than aqueous flood

deposits [*Hamilton et al.*, 2010c]. On the basis of spatial distribution of VRC analogs, lava thickness associations, and thermodynamic modeling of lava-substrate heat transfer, *Hamilton et al.* [2010c] concluded that the volatile source for rootless eruptions in the western Tartarus Colles region could have been an obliquity-controlled ground ice reservoir located at depths of several tens of meters or less. If so, then it appears that explosive lava-water interactions on Mars can involve atmospheric sources of water and do not necessarily imply an association with aqueous floods.

2.3. VRC Archetypes

[9] Studies of explosive lava-water interactions have largely focused on the morphological characteristics of terrestrial VRCs and comparisons to analogous structures observed within Mars satellite imagery. Early investigations of VRCs in Iceland [e.g., *von Komorowicz*, 1912; *Rittman*, 1938; *Thorarinsson*, 1951, 1953] documented many morphological complexities within terrestrial rootless cone groups. However, since then studies have generally focused on the radially symmetric crater-in-cone structures found in the vicinity of Lake Mývatn in Iceland because of their accessibility and resemblance to the VRC analogs that were first discovered on Mars. The crater:cone diameter ratio has become the most widely used morphological parameter in the description of VRCs on Earth and their analogs on Mars [e.g., *Frey and Jarosewich*, 1982; *Greeley and Fagents*, 2001; *Fagents et al.*, 2002; *Sheth et al.*, 2003; *McGowan*, 2009], but the use of this metric presupposes that this ratio is a characteristic property of landforms generated by explosive lava-water interaction. However, this is unrealistic given the morphological variability of VRCs in Iceland [e.g., *Thordarson et al.*, 1998; *Fagents and Thordarson*, 2007; *Hamilton et al.*, 2010a, 2010b]. Moreover, *Fagents et al.* [2002] observed that direct comparisons between crater: cone diameter ratios for VRCs on Earth and Mars could be misleading because of the effects of differing gravity and atmospheric pressure on eruption processes in these two planetary environments. *Hamilton et al.* [2010a] introduced a series of commonly occurring morphological forms (i.e., archetypes) that depend primarily upon the intensity and duration of the rootless eruption activity, location and structure of lava pathways, proximity of rootless eruption sites to each other, and the nature of the surface upon which rootless tephra is deposited.

[10] If explosive lava-water interactions disperse tephra radially onto stationary lava surfaces, then the resulting VRCs can include three primary archetypes: isolated cratered cones with radial symmetry [e.g., *Jurado-Chichay et al.*, 1996]; elongated VRCs composed of linearly aligned cratered cones [e.g., *Fagents and Thordarson*, 2007]; and irregularly shaped rootless tephra complexes composed of interfingered pyroclastic deposits from numerous explosion sites [e.g., *Thordarson et al.*, 1998]. Radially symmetric cratered cones are typically fed by internal lava pathways (e.g., lava tubes) with tephra accumulating without interference from nearby rootless eruption sites. If multiple rootless eruptions occur along a lava tube, then adjacent radially symmetric cratered cones can overlap to form composite structures with elongated morphologies. Rootless tephra complexes are also composed of tephra erupted from multiple rootless eruption sites, but they are fed from broad sheet-like lobes, rather than narrow tubes, and thus do not tend to exhibit morphologies with strong linear alignments [*Hamilton et al.*, 2010a].

[11] In contrast, if rootless tephra is deposited onto a moving lava surface, then tephra can be rafted away from the depocenter of the rootless eruption site to create partial cones, such as paired half-cones on either side of active lava channels [e.g., *Fisher*, 1968; *Fisher and Schmincke*, 1984]. Rootless eruptions can also construct asymmetrical tephra deposits on stable surfaces located along the margins of broad zones of lava surface motion [*Hamilton et al.*, 2010a]. Elongated VRCs in the Laki lava flow in Iceland occur where fixed rootless eruption sites have deposited tephra onto moving lava surfaces [*Hamilton et al.*, 2010a, 2010b] and are analogous to those identified on Mars by *Jaeger et al.* [2007, 2010], *Keszthelyi et al.* [2010], and *Hamilton et al.* [2010c].

[12] On Mars, elongated VRCs also include chains of raised rim craters that are aligned in the direction of lava flow surface motion. These structures are interpreted to have formed during rootless eruptions involving cyclical explosions with rootless tephra deposits from each explosion event being rafted downflow. Similar VRC morphologies have not yet been discovered on Earth, but well-defined chains of lava-rafted pyroclastic material are common within Martian cone groups in Athabasca Valles and the Tartarus Colles region [*Jaeger et al.*, 2007, 2008; *Hamilton and Fagents*, 2009; *Keszthelyi et al.*, 2010]. High-resolution (25–32 cm/pixel) imagery from the MRO HiRISE camera have also revealed other VRC morphologies that have not been described on Earth [*Jaeger et al.*, 2007, 2008, 2010; *Keszthelyi et al.*, 2010]. These archetypes include cratered cones with surrounding "moats" that formed by the flexure and failure of lava crusts loaded by rootless tephra [*Jaeger et al.*, 2007, 2008, 2010; *Keszthelyi et al.*, 2010] and preferential VRC concentrations above the rims of lava-mantled impact craters and yardangs [*Keszthelyi et al.*, 2010].

[13] *Keszthelyi et al.* [2010] also describe pitted terrains on Mars, which they interpret as the products of lava-induced sublimation of ground ice and subsequent overburden collapse [*Keszthelyi et al.*, 2008, 2010]. Although pitted terrains are not produced by rootless eruptions, they can be associated with VRCs and provide evidence of lava–ground ice interactions.

2.4. Geospatial Analysis of VRCs on Mars

[14] *Bruno et al.* [2004, 2006] were the first to introduce nonmorphological criteria to validate the Martian VRC hypothesis. These studies compared a variety of geological features on Earth and Mars (e.g., VRCs, ice-cored mounds, and secondary impact craters) using nearest neighbor (NN) analyses [*Clark and Evans*, 1954] and demonstrated that most of the conical landforms that had been interpreted as VRCs and pingos on Mars are clustered relative to a Poisson (i.e., random) model and their spatial distributions are statistically indistinguishable from the patterns displayed by terrestrial VRCs. Among the 10 Martian test cases investigated by *Bruno et al.* [2006], the only exception occurs within Gusev Crater. Within this region, a group of mounds (considered to be pingos by *Cabrol et al.* [2000]) have greater than random (i.e., repelled) nearest neighbor (NN) distances and exhibit lava flow associations that led *Bruno et al.* [2006] to reinterpret them as secondary impact craters that

had been inundated by lava and then topographically inverted by lava flow inflation.

[15] *Baloga et al.* [2007] reexamined a cone group in the western Tartarus Colles region using a sample-size-dependent NN analysis technique and a methodology that removed spatial outliers from the input distribution. Their results differed from those of *Bruno et al.* [2004, 2006] by showing that VRC analogs on Mars can exhibit statistically significant repelled distributions. *Bishop* [2008] also examined the geospatial distribution of cones in the western Tartarus Colles region using higher-order NN analyses and determined that the landforms generally exhibit spatial randomness across all distance scales extending to sixth-order neighbors, except within regions that have undergone erosional modification. In some of these modified regions, NN distributions exhibit statistically significant clustering relative to a Poisson model.

[16] These contrasting results raise issues regarding the utility of NN analysis as a remote sensing tool and as a metric for the nonmorphological comparison of landforms. For instance, rootless eruption sites among the Hnúta and Hrossatungur groups in Iceland show that relative to a Poisson distribution, NN distances can range from repelled to random for small sample sizes, whereas larger populations of rootless eruption sites tend to be clustered [*Hamilton et al.*, 2010b]. Thus a single NN statistic cannot provide unambiguous evidence to prove or disprove the identity of VRCs. Nonetheless, NN statistics can be used to identify nonrandom structures within geologic systems and provide insight into geologic processes such as resource heterogeneity and self organization through competitive utilization of limited resources. However, to meaningfully interpret NN statistics and compare results from different studies, it is important to carefully consider the assumptions that are made in each analysis. Section 5.4.3 demonstrates how understanding the influences of different model parameters can largely reconcile the variations in geospatial distribution that have been reported for rootless eruption sites on Earth and Mars [e.g., *Bruno et al.*, 2004, 2006; *Baloga et al.*, 2007; *Bishop*, 2008; *Burr et al.*, 2009a; *Hamilton et al.*, 2010b; this study].

2.5. Numerical Models of VRC Formation

[17] To date, studies of VRC formation have been largely conceptual, with notable exceptions being numerical models of rootless tephra dispersal [e.g., *Greeley and Fagents*, 2001; *Fagents et al.*, 2002] and lava-substrate heat transfer [e.g., *Squyres et al.*, 1987; *Wilson and Head*, 2007; *Hamilton et al.*, 2010c]. The tephra disperal models of *Greeley and Fagents* [2001] and *Fagents et al.* [2002] considered the physical effects of atmospheric pressure, gravity, and volatile abundance on the dispersal of ballistic pyroclasts generated by transient rootless explosions. These numerical simulations established theoretical constraints on the substrate volatile contents that were required to produce rootless cones of a given diameter under different planetary conditions, and they demonstrated that Martian rootless cones could have been produced by explosive lava-water interactions involving plausible abundances of ground ice.

[18] Existing thermodynamic models of lava-substrate heat transfer significantly oversimplify the complex mechanisms of lava flow field growth by assuming that the duration of the lava emplacement is negligible relative to the total cooling history of the flow. Nevertheless, these models help to describe the effects that cooling lava flows can have on their surroundings. For instance, *Squyres et al.* [1987] developed models of volcano–ground ice interactions on Mars that describe both lava flow emplacement over ice-rich permafrost and sill intrusions into ice-bearing permafrost. For lava flow emplacement over permafrost substrates with 25% ground ice and plausible ambient temperature and pressure conditions for Mars, *Squyres et al.* [1987] determined that the maximum depth of ground ice melting would be approximately 1.5–2 times the lava flow thickness. For glacial environments on Earth, *Wilson and Head* [2007] modeled conductive heat transfer between basaltic magmas and their surroundings during the emplacement of supraglacial and subglacial lava flows, as well as dike injections into glaciers. Instead of considering only pure ice and lithic substrates, *Hamilton et al.* [2010c] expanded upon *Wilson and Head* [2007] by modeling conductive heat transfer between basaltic lava flows and ice-bearing substrates with 0–30% ice content. *Hamilton et al.* [2010c] also ran their simulations over a range of ambient temperature conditions that represent permafrost environments on both Earth and Mars. In their baseline scenario for Mars, *Hamilton et al.* [2010c] showed that ground ice could be melted in the substrate to maximum depths that are ~2.2 times the lava flow thickness, but at the time when the core of the basaltic lava flow reaches 1273 K, the maximum ice melting depths would only be ~0.6 times the lava flow thickness. *Hamilton et al.* [2010c] considered the 1273 K isotherm to be significant because it approximates the temperature at which basaltic lava would become too viscous to dynamically mix with external water and generate explosive molten fuel-coolant interactions (MFCIs). Therefore, in permafrost environments on Mars, the upper bound on the amount of water that would be available to participate in explosive lava-water interactions would be defined by the maximum extent of ground ice melting that could occur prior to the lava core temperature reaching ~1273 K. In section 6.1 we return to the topic of lava-substrate heat transfer in greater detail to constrain a model for the formation of VRCs and thermokarst within the Tartarus Colles volcanic unit.

3. Study Location, Methodological Approaches, and Preprocessing Results

[19] The Tartarus Colles cone groups, including both the eastern and western groups, are located on Mars between northeastern Elysium Planitia and southern Arcadia Planitia (25°N–28°N, 165°E–190°E). This region is located where several channel systems debouch onto the northern plains [*Keszthelyi et al.*, 2010; *Hamilton et al.*, 2010c]. *Tanaka et al.* [2005] attribute all of the lava flows in the Tartarus Colles region to the early Amazonian to late Hesperian age Elysium rise unit, but among these flows, *Hamilton et al.* [2010c] identified a stratigraphically younger VRC-hosting volcanic unit with a model age of ~75–250 Ma (i.e., late to middle Amazonian). This model age represents an estimated crater retention age of 125 Ma with a factor of ±2 uncertainty based on the Martian crater-count isochron diagram of *Hartmann* [2007].

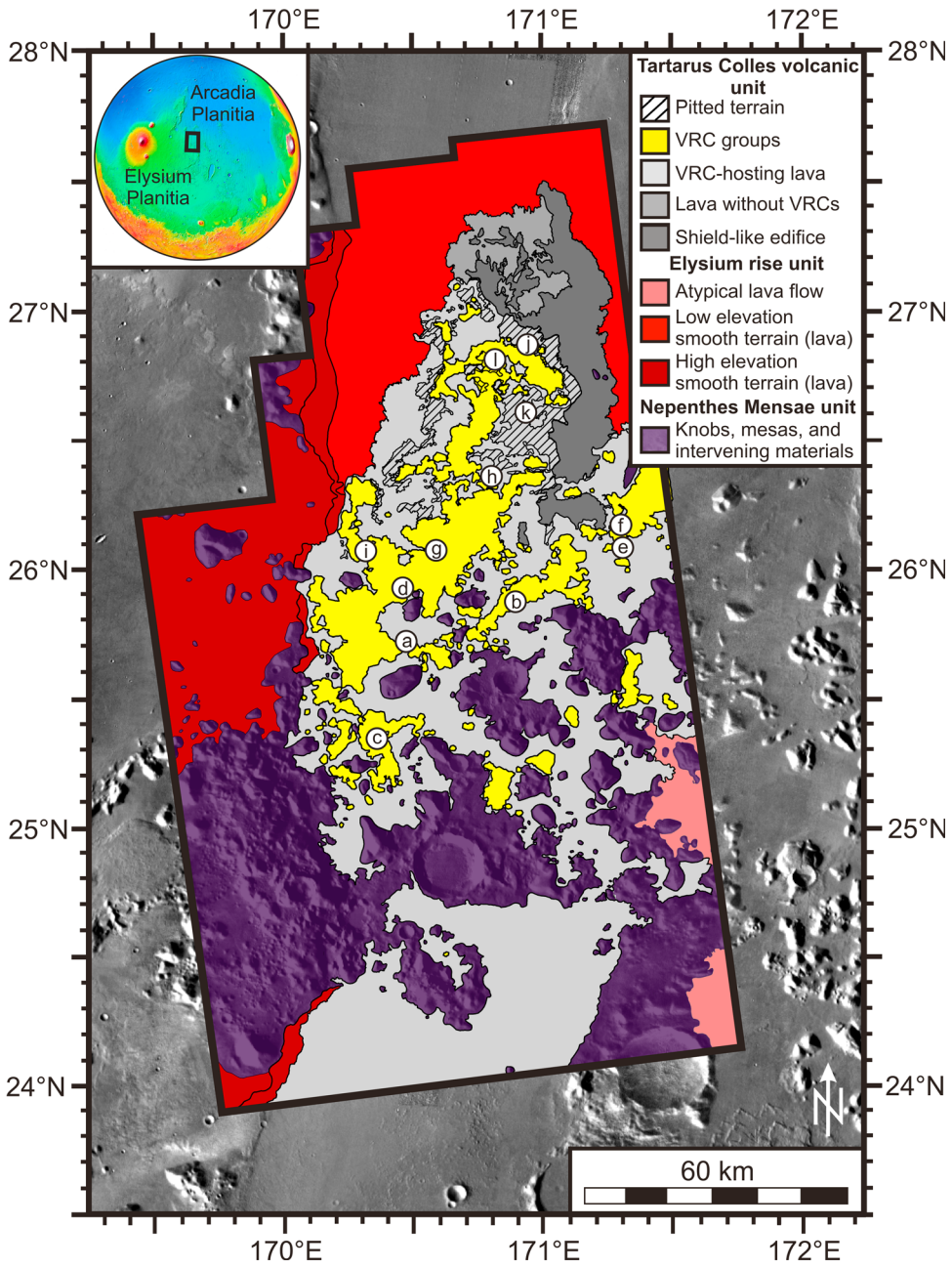

Figure 1. Inset shows study area location between Elysium Planitia and Arcadia Planitia; warm colors represent high elevations, whereas cool colors represent low elevations. Boundaries of the geological map are defined by current limits of Mars Reconnaissance Orbiter (MRO) CTX image coverage. Volcanic rootless construct (VRC) group boundaries are defined using a threshold of 10 rootless eruption sites per square kilometer (see Figure 2). Circled labels a–l refer to locations of the images shown in Figure 3.

[20] Our study involves morphological and geospatial analyses of landforms in the western portion of the Tartarus Colles region (Figure 1) using a geospatial database in ArcGIS with a basemap mosaic consisting of 12 MRO HiRISE images, 11 MRO CTX images, and 19 MGS MOC narrow angle images located in a region spanning from approximately 24°N–28°N and 169°E–172°E. Additional Mars Odyssey Thermal Emission Imaging System (THEMIS) visible and daytime infrared images were used for regional context, but are of insufficient resolution to reliably identify VRCs. *Hamilton et al.* [2010c] used the same image database to develop photogeological maps of the Tartarus Colles region, but in this study we improve upon their mapping by adding new "pitted terrain" facies within the Tartarus Colles volcanic unit and by digitizing the locations of 40,004 putative rootless eruption sites. Digitization of rootless eruption sites as point features allows us to obtain population density information, quantify patterns of spatial distribution among

rootless eruption sites using nearest neighbor (NN) analysis, and determine the relationship between rootless eruption site locations and the thickness of the Tartarus Colles lava flow.

[21] We distinguish between VRCs and rootless eruption sites in that VRCs are the depositional products of rootless eruptions [*Fagents and Thordarson*, 2007], whereas rootless eruption sites are the surface projections of underlying explosion centers. We assume that the centroid of each VRC crater corresponds to a rootless eruption site and, consequently, if VRCs exhibit multiple craters, we define multiple rootless eruption sites within them. In instances where it is apparent that rootless tephra has been rafted downflow by lava surface motion, we do not digitize apparent rootless eruption sites in the elongated crater ramparts because they have been displaced from their original locations.

[22] To define domains of rootless eruption sites within the Hnúta and Hrossatungur groups of the Laki lava flow in Iceland, *Hamilton et al.* [2010a, 2010b] used a combination of field-based stratigraphic, tephrochonological, and geospatial evidence to isolate regions in which rootless eruptions occurred contemporaneously. Within the Tartarus Colles region, these lines of evidence are not available, and so to isolate domains that can be meaningfully compared to those documented on Earth, we must rely upon remote sensing and geospatial analysis. Using the ArcGIS "Point Density" tool, we calculated the number of rootless eruption sites per square kilometer in each cell using an output cell size of 100 m and a circular neighborhood with a radius of 564 m. Resulting densities range from 0 to 277 rootless eruption sites per square kilometer (Figure 2). A threshold of 10 rootless eruption sites per square kilometer was then applied to the density map to identify 76 continuous subregions within the Tartarus Colles groups. This threshold was chosen because it provided the best agreement with the manually delimited VRC domain boundaries presented by *Hamilton et al.* [2010c]. Locations of all rootless eruption sites in each domain were extracted as tables of object coordinates and filtered to remove VRC domains with <30 rootless eruption sites because data sets with fewer than ~30 objects rarely generate meaningful NN statistics [*Bruno et al.*, 2006]. Rootless eruption site locations in the remaining 36 domains were analyzed using the NN module of GIAS version 1.12 [*Beggan and Hamilton*, 2010], with renormalized Poisson analyses employing a detection threshold of r_0 = 6 m. Section 5 elaborates on our NN methodology and choice of threshold values.

[23] To estimate the thickness of the Tartarus Colles lava flow, we subtracted a local datum from MGS Mars Orbiter Laser Altimeter (MOLA) Mission Experiment Gridded Data Record (MEGDR) at 128 pixel/degree resolution (0°N–44°N, 90°E–180°E). North of 26°N, this method is justified because the Tartarus Colles lava flow debouches onto the northern plains and the lava directly overlies a smooth terrain with an exposed surface slope of only 0.03° to 0.09° [*Hamilton et al.*, 2010c]. We assume that the smooth terrain projects beneath the Tartarus Colles lava flow and model the underlying surface as an inclined plane with a constant slope of 0.05° and a constant vertical offset that provides a best fit to the elevation of the exposed portion of the smooth terrain. By subtracting our local datum from MOLA topography, we obtain an elevation thickness residual, which is used to characterize lava thickness distributions. Unexpected variations in the underlying topography could affect our estimated lava thicknesses, but this is why we have restricted our attention to the region that is adjacent to the exposed surface of the smooth terrain, which is far removed from the influences of the high-relief Nepenthes Mensae unit.

[24] To estimate the thickness distribution of the Tartarus Colles lava flow, we sampled the lava thickness raster using the "Extract by Polygon" tool in ArcGIS and a shape file representing the extent of the Tartarus Colles lava flow. Similarly, to estimate the thickness of the Tartarus Colles lava flow at each rootless eruption site and within the pitted terrain regions, we sampled the lava thickness raster using ArcGIS "Sample by Point" and "Extract by Polygon" tools, which employed shape files containing the locations of rootless eruption sites and pitted terrain boundaries, respectively. The resulting lava thickness distributions are presented in section 5.3.

4. Morphological Analysis

4.1. Geology of the Western Tartarus Colles Region

[25] The western Tartarus Colles region includes three main geological units (Figure 1): the Nepenthes Mensae unit, the Elysium rise unit, and the Tartarus Colles volcanic unit. The Nepenthes Mensae unit is of early Hesperian to early Noachian age and is exposed within the high-standing knobs and mesas of the Tartarus Colles [*Tanaka et al.*, 2005]. The Elysium rise unit is of early Amazonian to late Hesperian age and consists of lava flows that were erupted from Elysium Mons, Hecates and Albor tholi, and local sources [*Tanaka et al.*, 2005]. In Figures 1 and 2 we subdivide the Elysium rise unit into high-elevation smooth terrains, low-elevation smooth terrains, and anomalous lava flows. The high-elevation smooth terrain is composed of lava flows that form an approximately north-south trending barrier of high topography that is located along the western margin of the study area. Low-elevation smooth terrain is also composed of lava flows, but they are mantled by sedimentary deposits that thicken toward the west [*Hamilton et al.*, 2010c].

[26] Along the southeast margin of the study area are two lava flow surfaces, which we describe as anomalous because they have flow directions that are atypical of other lavas in this sector of Elysium Planitia [*Hamilton et al.*, 2010c]. *Tanaka et al.* [2005] do not differentiate these flows from the Elysium rise unit, but we suspect that this lava moved northward through valleys incised into the Nepenthes Mensae unit and that these lava branches may be associated with the Tartarus Colles volcanic unit. However, higher-resolution data (e.g., CTX imagery) are required to confirm this hypothesis.

[27] The Tartarus Colles volcanic unit directly overlies the low-elevation smooth terrain of the Elysium rise unit and includes five principal facies (Figure 1): a shield-like edifice, a lava flow without VRCs, a VRC-hosting lava flow field, VRC groups, and pitted terrains. The interpretation that cratered cones within the Tartarus Colles region are VRCs was suggested by previous investigators [e.g., *Greeley and Fagents*, 2001; *Lanagan et al.*, 2001; *Fagents et al.*, 2002; *Bruno et al.*, 2004, 2006, *Baloga et al.*, 2007; *Fagents and Thordarson*, 2007; *Hamilton et al.*, 2010b, 2010c; *Keszthelyi*

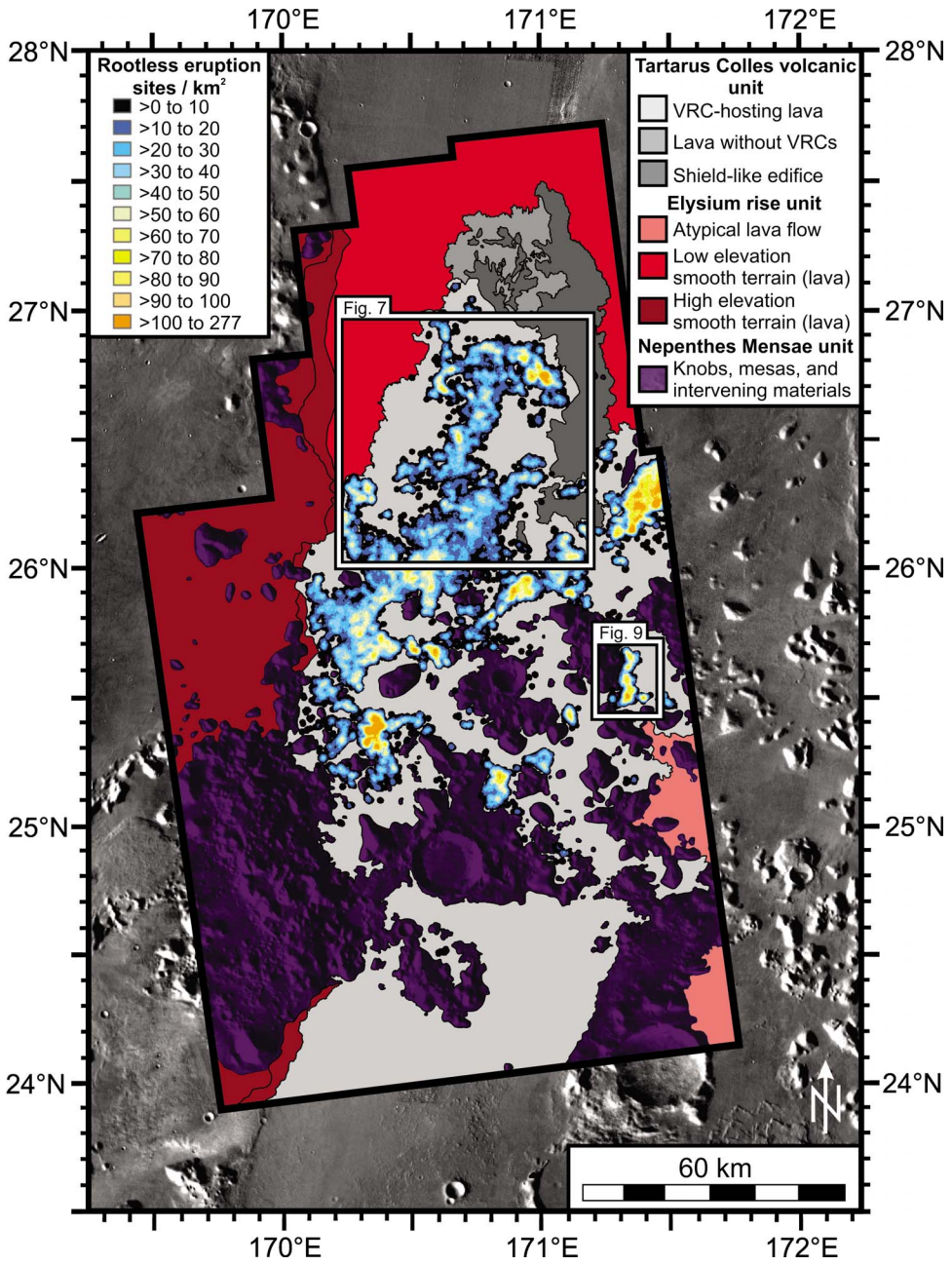

Figure 2. Rootless eruption sites in the western Tartarus Colles region. Population densities calculated for 100 m wide cells using a database of 40,004 rootless eruption sites and a search radius of 564 m. The population density map shows that rootless eruption sites concentrate where the Tartarus Colles lava flow debouches onto the smooth terrain after emerging from the confinement of the Nepenthes Mensae unit. Insets show the locations of Figures 7 and 9.

et al., 2010], but in this study we explore new morphological and geospatial evidence to evaluate this hypothesis.

[28] The shield-like edifice in the Tartarus Colles volcanic unit exhibits inflated pahoehoe margins and a degraded surface that slopes away from a north-south trending axis [*Hamilton et al.*, 2010c]. The northwestern parts of the shield-like unit are largely overlain by smooth lava flows that do not include VRCs, whereas along its southern margins, the shield-like edifice is overlain by the VRC-hosting portion of the Tartarus Colles lava flow. The origin of the shield-like edifice is ambiguous, but its location and morphology suggest that it is a rootless shield [*Kauahikaua et al.*, 2003] that was fed by breakouts from a northward flowing lava pathway. Thus we consider the edifice to be an early component of the Tartarus Colles lava flow field, rather than a part of the Elysium rise unit. The VRC-hosting lava flowed northward from Elysium Planitia through a network of valleys in the Tartarus Colles. A source region cannot be unambiguously identified, but the flow appears to originate from the vicinity of Grjótá Valles. Figure 2 shows the

population density of rootless eruption sites in the western Tartarus Colles region and illustrates that VRCs concentrate primarily in lava that debouched onto the low-elevation smooth terrain after it emerged from the confinement of the Nepenthes Mensae unit. The study area includes 180 cone groups with a total area of ~2000 km^2 [*Hamilton et al.*, 2010c]. However, these values are minimum estimates for the number and total area of the VRC groups in the western Tartarus Colles region because additional groups are located in the eastern part of the lava flow, which extends beyond the region of continuous CTX image coverage.

4.2. Description of Landform Characteristics in the Tartarus Colles Volcanic Unit

4.2.1. Radially Symmetric Cratered Cones

[29] Cratered cones in the Tartarus Colles region tend to be either radially symmetric (e.g., Figures 3a–3c and 4a and 4b) or elongated (e.g., Figures 3d–3f and 4c and 4d). Radially symmetric cones can occur in isolation (e.g., SE corner of Figure 3a) and as composite structures (e.g., center of Figure 3a). They directly overlie lava flow surfaces, have approximately circular geometries in plan view, and include a positive relief conical edifice surrounding a central crater. All radially symmetric cratered cones in the study region are located within the Tartarus Colles lava flow.

[30] The apparent roughness of the lava decreases toward the cones, which have basal diameters ranging from tens to hundreds of meters. The flanks of the cones dip radially outward and commonly exhibit darker streaks on their outer slopes. Crater walls have steep inward dipping slopes that can include darker overhanging protrusions. Inner crater walls are commonly layered and appear blocky. Crater floors are typically smooth but can include dark blocky material located near the base of the surrounding crater walls.

[31] Cones with approximate radial symmetry commonly contain multiple central depressions. In some instances, quasi-circular depressions within conical edifices can cross-cut other depressions to form perched craters, or develop elongate composite depressions where two or more circular depressions overlap without an evident superpositioning relationship. In such instances, there tends to be a general radial symmetry about each depression, even though the overall structure may be asymmetrical.

4.2.2. Elongated Cratered Cones

[32] Putative VRCs with elongated morphologies generally form fork-shaped positive relief structures composed of two subparallel branches that join at one end. The elongated VRCs have lengths ranging from tens of meters to kilometers (Figures 3d–3f and 4c and 4d). Like the radially symmetric cones, all elongated cones in the study area directly overlie the surface of the Tartarus Colles lava flow with apparent lava roughness decreasing toward the fork-shaped edifices. The subparallel branches of the forks form continuous structures that are thickest where they join in the form of a crescent. However, crescent-shaped connections between some forked branches are overprinted by radially symmetric cratered cones. Continuous layers can be observed in the inner walls of some of the fork-shaped structures, where dark layers protrude from the surrounding light-toned material.

[33] The fork-shaped structures are commonly found together with chains of aligned raised-rim craters that extend for several hundred meters (Figure 3d–3f). These raised-rim structures each exhibit a central depression and have basal diameters of several tens of meters. Like the fork-shaped structures, the raised-rim crater chains tend to be open at one end and include radially symmetric cones at the other end. The axes of adjacent elongated structures, including both fork-shaped and raised-rim crater chains, generally exhibit parallel orientations.

4.2.3. Annular Arrangements of Cratered Cones

[34] Within the Tartarus Colles cone groups, there are several ring-shaped structures composed of radially symmetric cratered cones (Figures 3g–3i). These ring structures have diameters of ~0.5–1.5 km. Cratered cones are not observed within the interior of the rings, whereas outside of the rings, there tends to be a paucity of cones in a zone extending for several hundred meters. Beyond this low population density zone, the frequency of cratered cones increases and becomes consistent with the average population density in the cone groups (Figure 2).

4.2.4. Pitted Terrain

[35] Throughout the Tartarus Colles lava flow there are numerous regions of pitted terrain that show a close spatial association with the cratered cones (Figures 3j–3l). These pitted terrains typically include numerous depressions with intervening septa composed of darker blocky material. In plan view, their shapes range from approximately circular to sinuous and highly irregular. The depressions appear to dissect previously continuous lava surfaces and overlying cones to form high-standing islands of lava that are entirely surrounded by pitted terrain. The MOLA 128°/pixel MEGDRs show that elevation differences between pitted terrains and surrounding lava surfaces are <20 m. Figure 3j shows a cone-hosting lava surface that grades into a pitted terrain with a blocky surface, Figure 3k shows examples of cratered cones in the center of a pitted terrain, and Figure 3l shows part of a VRC-covered region exhibiting subdued pit-like forms within a cone group.

4.3. Interpretation of Landform Characteristics in the Tartarus Colles Volcanic Unit

4.3.1. Radially Symmetric Cratered Cones

[36] Radially symmetric cratered cones in the western Tartarus Colles region exhibit four concentric morphological facies: distal sheet, intermediate platform, proximal cone, and central crater. In the vicinity of cratered cones, the distal sheet facies forms a light-toned deposit that partially mantles the darker surface of the Tartarus Colles lava flow. We note that the apparent contrasts in tone could result from variations in surface roughness with finer-grained material appearing brighter than rougher surfaces that may include internal shadows. The distal facies grades inward into a thicker platform facies that obscures most of the roughness of the underlying lava surface. The platform facies in turn thickens toward the cones. The outer flanks of the cones generally appear smooth and light toned, except for where darker slope streaks are present. The slope steaks widen downdip and are morphologically similar to those identified elsewhere on Mars by *Sullivan et al.* [2001]. *Sullivan et al.* [2001] interpret the slope streaks to be the products of granular flows of unconsolidated sediments (i.e., dust avalanches) that have revealed a darker and/or rougher underlying surface. This interpretation is consistent with our observations;

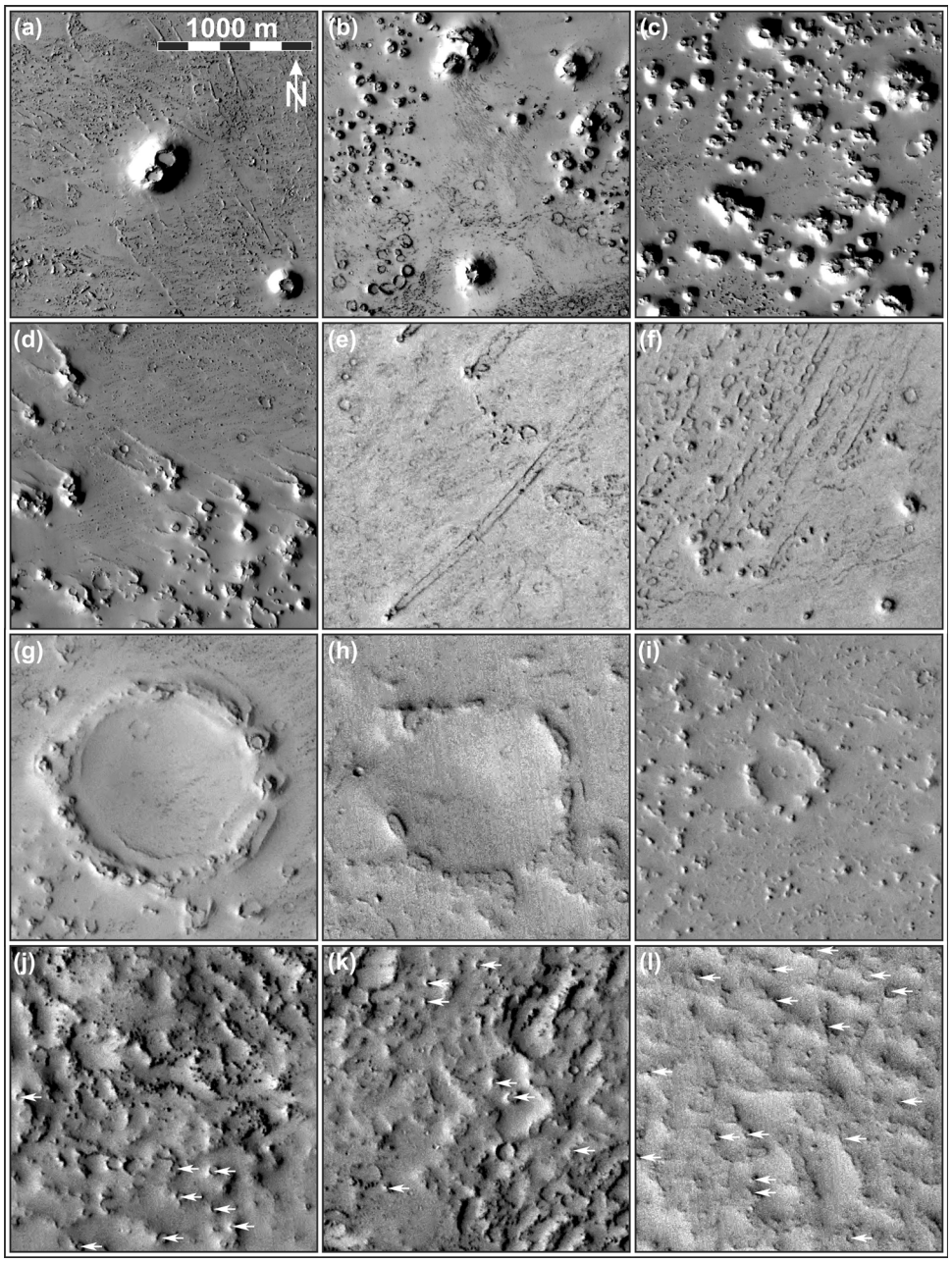

Figure 3. Volcanic rootless constructs (VRCs) and related terrains in the western Tartarus Colles region. All images are illuminated from the west, are oriented with north toward top, and have the same scale. (a–c) Examples of radially symmetric cratered cones with some tephra complexes formed by interfingered deposits from multiple sources. (d–f) Asymmetrical cratered cones elongated in the direction of lava surface motion at the time of emplacement. Flow directions were approximately NW in Figure 3d and NE in Figures 3e and 3f. (g–i) Annular arrangements of cratered cones. (j–l) Pitted terrains associated with cratered cones. A selection of VRCs in Figures 3j–3l are indicated by white arrows, but to maintain legibility not all VRCs in these images have been labeled. Figures 3a–3d are extracted from HiRISE imagery, whereas Figures 3e–3l are from CTX images. The corresponding image identification numbers are Figure 3a, PSP_008528_2060; 3b, PSP_007671_2065; 3c, PSP_003900_2055; 3d, PSP_002344_2065; 3e and 3f, P14_006669_2050_XN_25N188W; 3g and 3i, P03_002344_2067_XN_26N189W; 3h, P07_003900_2050_XI_25N189W; 3j and 3l, P03_002344_2067_XN_26N189W; and 3k, P18_008027_2071_XN_27N188W.

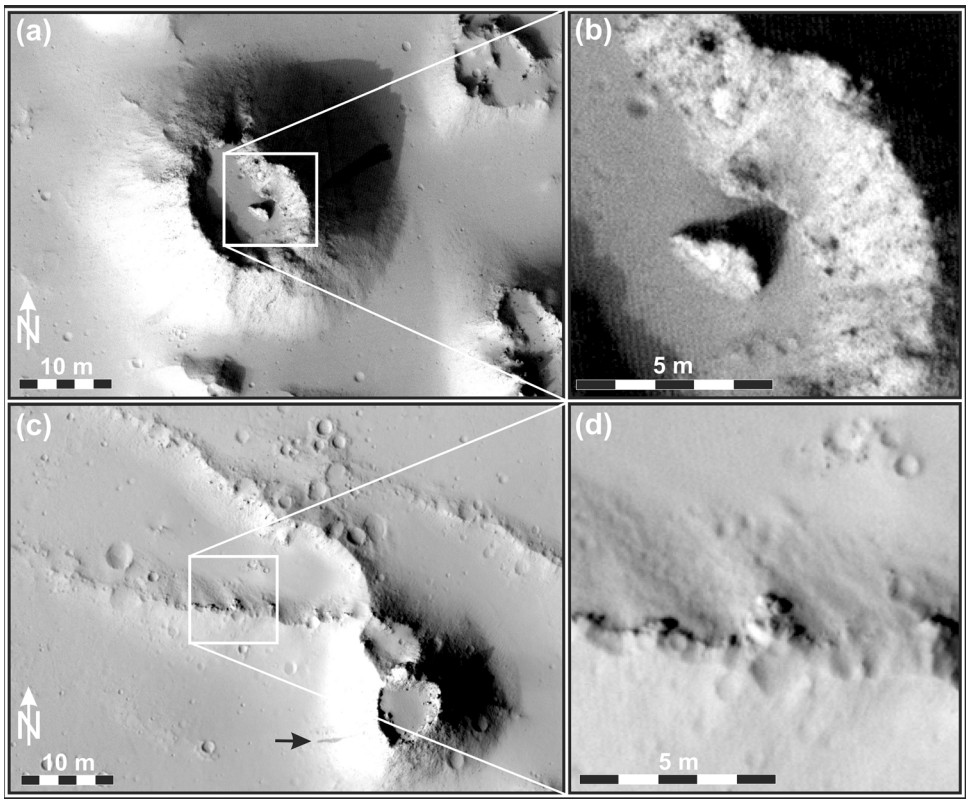

Figure 4. HiRISE images of VRCs within the Tartarus Colles cone groups. (a and b) Parts of PSP_003900_2055 (30 cm/pixel, subsolar azimuth 137.8°) showing a radially symmetric cratered cone with a competent collapse block in its central crater. (c and d) Parts of PSP_002344_2065 (30 cm/pixel, subsolar azimuth 165.5°) showing a downflow elongated cratered cone with a fork-shaped morphology that exhibits a continuous competent layer. In Figures 4c and 4d the lava flow direction is inferred to have been toward the NW with two rootless eruption sites initiating after the lava flow surface came to rest to generate the radially symmetric cones at the SSE end of the structure. Arrow identifies a dark slope streak.

thus we infer that the slope streaks are the products of mass movements that have affected oversteepened aeolian sediments on the outer flanks of the cones. Central craters have walls composed of competent material with overhanging projections and steep slopes that exceed the angle of repose for dry unconsolidated granular materials. Given that downslope (i.e., driving) and normal (i.e., resisting) forces are both proportional to gravity, *Burr* [2005] concludes that the angle of repose on Earth and Mars should be similar (i.e., ~25°–40° [*Selby*, 1993]). Thus steeply sloping and overhanging material observed in the central craters suggest that the crater walls are at least partially composed of competent material. Additional support for this interpretation is provided by the presence of meter-scale blocks within central craters. For instance, the block shown in Figures 4a and 4b suggests that material collapsed from the crater wall onto the smooth surface of the crater floor. This implies that crater rim deposits were sufficiently competent to undergo brittle failure and that the blocks were strong enough to retain their shape during and after the collapse.

[37] The facies associations observed among the radially symmetric cratered cones in the western Tartarus Colles region are consistent with those documented for VRCs on Earth [*Thordarson et al.*, 1998; *Fagents and Thordarson*, 2007; *Hamilton et al.*, 2010a]. *Fagents and Thordarson* [2007] attribute these stratigraphic sequences to repeated cycles of explosive fragmentation and tephra dispersal, with rootless eruption intensity generally decreasing with time as external water is depleted relative to available molten lava [*Fagents and Thordarson*, 2007]. As the rootless eruption progresses, this results in less thorough fragmentation, larger clasts, and lower eruption velocities, which in turn lead to an increasingly large proportion of erupted material being contributed to the proximal conical edifice, at the expense of the more distal facies.

[38] On the basis of the observed facies associations, we interpret the radially symmetric cratered cones in the western Tartarus Colles region to be VRCs that were produced by explosive lava-water interactions. Additionally, we conclude that the competent material exposed in the crater walls is analogous to the spatter-rich tephra deposits that are generated during late-stage (i.e., water-limited) rootless eruptions on Earth [*Fagents and Thordarson*, 2007; *Hamilton et al.*, 2010a]. If late-stage rootless explosions formed indurated deposits as spattery clasts agglutinated together [*Jaeger et al.*, 2007], then the partially molten state of the spatter implies that the explosive lava-water interactions occurred before the core of the Tartarus Colles lava flow solidified.

4.3.2. Elongated Cratered Cones

[39] Radially symmetric VRCs are circular in plan view because they are constructed by rootless explosions that disperse tephra radially onto stationary surfaces [*Thorarinsson*, 1951, 1953]. In contrast, fork-shaped VRCs on Earth are elongated because radially dispersed tephra is deposited onto moving lava surfaces that raft material away from its source [*Hamilton et al.*, 2010a]. By analogy, we attribute the subparallel branches of the fork-shaped deposits in the western Tartarus Colles region to explosive lava-water interactions that emplaced tephra onto moving lava surfaces.

[40] Lava rafting of pyroclastic material exposes the oldest components of elongated VRCs at the downflow end of the structures, with deposits becoming progressively younger toward their eruption source and at higher stratigraphic levels. If a lava surface is moving and the explosion intensity of a rootless eruption gradually wanes, then deposits will become progressively less widely dispersed, thicker, and increasingly spatter-rich in the vicinity of rootless eruption sites. Thicker proximal tephra deposits would also be favored by decreasing lava flow surface velocities, which would provide surfaces with more time to accumulate tephra before they were rafted away from the depocenter. Fork-shaped edifices grade outward into platform and sheet facies, whereas the inner walls of the subparallel branches dip toward the former location of the vent and thin in the direction of flow. Outer slopes of the fork-shaped branches and inner margins of elongated crater ramparts are analogous to outer slopes and crater walls of radially symmetric cratered cones, respectively. Thus, despite differences in their morphology, radially symmetric VRCs and elongated VRCs tend to exhibit similar facies associations because they are formed by similar explosion processes.

[41] In some instances, elongated VRCs can include one or more radially symmetric cratered cones at their upflow end. The radial symmetry of these late-stage constructs implies that lava surface motion ceased during the eruption. Figure 4c provides an example of one such VRC structure. On the basis of the axis of elongation, tapering width, and increasing thickness of the VRC, we infer that at this locality the lava surface was moving toward the NW when the rootless eruption initiated and that the explosion intensity waned with time. Diminishing explosion intensity, decreasing tephra dispersal range, and increasingly spatter-rich deposits can be explained by a systematic decrease in the water:lava ratio as water was exhausted in the vicinity of the rootless eruption site [*Wohletz*, 1986, 2002]. However, in Figure 4c, the radially symmetric cratered cone located at the upflow end of the structure (i.e., the SE end) indicates that lava flow surface motion ceased before the end of the rootless eruption. Figure 3e shows an elongated VRC with continuous tephra ramparts that can be traced over 2 km NE from their source, which is marked by a radially symmetric cratered cone at the SW end of the structure.

[42] Our conceptual model for the formation of elongated VRCs agrees with the mechanisms proposed by *Jaeger et al.* [2007] for analogous landforms in Athabasca Valles. Consequently, elongated VRC examples provide compelling evidence to suggest that rootless eruptions occurred in the Tartarus Colles region before and after the underlying lava flow surface came to rest and that the lava and overlying cratered cones are associated with the same volcanic event.

4.3.3. Annular Arrangements of Cratered Cones

[43] Cratered cones that make up the ring-shaped structures in the western Tartarus Colles region (Figures 3g–3i) exhibit morphological characteristics and facies associations that resemble radially symmetric VRCs. We therefore interpret them to be the products of explosive lava-water interactions but infer that their locations were systematically controlled to produce annular structures. Similar distributions of VRCs have been identified within the Athabasca Valles flood lava and have been interpreted as the result of rootless eruptions preferentially above the crests of buried yardangs [*Jaeger et al.*, 2007] and the rims of lava-inundated impact craters [*Keszthelyi et al.*, 2010]. In this scenario, active lava flows transferred heat to an ice-bearing substrate and generated water vapor that migrated toward regions of higher substrate elevation, such as buried impact crater rims, thereby concentrating water vapor above highs in the underlying topopgraphy. These localities became preferred locations for the triggering rootless eruptions once the gas pressure exceeded the overburden pressure and mechanical strength of the lava. Our observations are consistent with those of *Jaeger et al.* [2007] and *Keszthelyi et al.* [2010]; therefore we interpret the annular arrangements of VRCs in the western Tartarus Colles cone groups to have resulted from the structural controls that were imposed on the initiation of rootless eruption sites by the presence of buried impact craters.

4.3.4. Pitted Terrain

[44] Pitted terrains located throughout the Tartarus Colles lava flow show a close spatial association with VRCs (Figures 3j–3l). The pitted terrains are lower than their surroundings and, unlike the cratered cones, are not constructional. Additionally, dark blocks exposed within the pitted terrain suggest that the depressions are collapse features formed by the failure of a competent material. These pitted terrains also dissect previously continuous lava surfaces to leave islands of high standing lava, which in some instances include overlying cratered cones. This suggests that pitted terrains postdate both the emplacement of the Tartarus Colles lava flow and the cratered cones.

[45] *Keszthelyi et al.* [2008, 2010] inferred that similar terrains formed by the intrusion of lava beneath ice-rich sediments, sublimation of the ice, and collapse of the overburden. However, our observations suggest that the pitted terrain at this location formed within solidified lava with locally overlying rootless tephra deposits. Collapsed material thus belongs to the Tartarus Colles volcanic unit and not an ice-bearing sedimentary deposit located above a lava flow. We therefore propose that pitted terrains in the western Tartarus Colles region are thermokarst structures generated after VRC formation due to lava-induced melting of ground ice that was located beneath the flow. In sections 5 and 6 we present geospatial evidence and thermodynamic constraints to explore this hypothesis.

5. Geospatial Analysis

5.1. Nearest Neighbor (NN) Analysis of Spatial Distribution

[46] *Clark and Evans* [1954] proposed a simple test for spatial randomness in which the actual mean nearest neighbor (NN) distance ($\bar{r}_a$) in a region of known population density

is compared to the expected mean NN distance ($\bar{r}_e$) for a randomly distributed population of equivalent density. Following *Clark and Evans* [1954], $\bar{r}_e$ and the expected standard error (σ_e) of a Poisson distribution are

$$\bar{r}_e = \frac{1}{2\sqrt{\rho_0}} \tag{1}$$

$$\sigma_e = \frac{0.26136}{\sqrt{N\rho_0}}, \tag{2}$$

where the input population density (ρ_0) equals the number of objects (N) divided by the area (A) of the feature field ($\rho_0 = N/A$). To determine if $\bar{r}_a$ follows a Poisson distribution, the following two test statistics (termed R and c) are used:

$$R = \frac{\bar{r}_a}{\bar{r}_e} \tag{3}$$

$$c = \frac{\bar{r}_a - \bar{r}_e}{\sigma_e}. \tag{4}$$

[47] If a test population exhibits a Poisson random distribution, R should ideally have a value of 1, while c should equal 0. Thus if $R \approx 1$, then the test population may have a distribution that is consistent with the null hypothesis (i.e., a Poisson model). In contrast, if $R \neq 1$, then the null hypothesis may not be supported. Furthermore, if $R > 1$, then the test population exhibits greater than expected (i.e., repelled) NN distances, whereas if $R < 1$, then the NN distances in the test case are more closely spaced than expected and are thus clustered relative to the Poisson model.

[48] To evaluate the significance of R and identify statistically significant departures from the null hypothesis at the 0.95 and 0.99 confidence levels, $|c|$ must exceed the critical values of 1.96 and 2.58, respectively [*Clark and Evans*, 1954]. However, these critical values implicitly assume large sample populations. *Jerram et al.* [1996] and *Baloga et al.* [2007] note that finite-sampling effects introduce biases into the variation of NN statistics that are significant for small populations ($N \lesssim 300$). Thus, to account for these biases in our NN analyses, we employ the method of *Baloga et al.* [2007], which uses sample-size-dependent thresholds of significance for R and c.

[49] Geological Image Analysis Software (GIAS [*Beggan and Hamilton*, 2010]) includes tests for Poisson, renormalized Poisson, scavenged Poisson $k = 1$, and scavenged Poisson $k = 2$, NN distributions. The Poisson index k describes the number of higher-order NNs participating in a resource scavenging process [*Baloga et al.*, 2007], and if $k = 0$, then the scavenged NN model simplifies to the standard Poisson model. These NN analyses employ sample-size-dependent thresholds of significance at 1 and 2 standard deviations (σ) for R and c [*Baloga et al.*, 2007] and the convex hull method for bounding feature fields [*Graham*, 1972; *Bruno et al.*, 2006].

[50] The convex hull method uses the minimum bounding perimeter of a set of points to calculate the area of a feature field, A_{hull}, and determine its interior population density, $\rho_i = N_i/A_{\text{hull}}$, where N_i refers to the number of points located within the convex hull. NN distances are then calculated by allowing interior points to search for NNs among all points in the distribution, including the convex hull vertices. However, objects forming the vertices of the convex hull are not permitted to search for their own NNs because their NN could be located outside the convex hull. The mean NN distance among the interior points then replaces $\bar{r}_a$ in equations (3) and (4), and ρ_i substitutes for ρ_0 in equations (5)–(8) below. There could also be situations in which an interior point is located very close to a convex hull boundary with its true NN located outside the convex hull. In such a case, excluding all points outside the convex hull region would increase the average NN distance among interior points, relative to the mean NN distance in an infinite domain. This effect would generally have the greatest influence on domains with small populations and/or highly elongate geometries because a larger proportion of the total number of points in the distribution could have their true NN located outside the convex hull. However, in this study, we used continuous context camera (CTX) mosaics to identify the locations of all distinguishable rootless eruption sites in the western Tartarus Colles region and constructed our domain boundaries from that information. Consequently, we do not expect there to be a significant number of unrepresented NN points located outside the extent of the convex hull boundaries.

[51] The convex hull method implicitly assumes that the convex hull region provides a finite sample of an infinite domain. However, if heterogeneities cause objects to concentrate within a subset of the convex hull region, then A_{hull} can deviate significantly from A, which is the area of the region that is actually covered by objects of interest. For instance, if A_{hull} is significantly greater than A, then objects may appear regionally clustered because the convex hull method assumes that objects can form at random anywhere within the convex hull. This means that relative to ρ_0, the lower value of ρ_i will lead to larger $\bar{r}_e$ and lower R because $\bar{r}_a$ remains constant. Such a result can provide insight into regional processes controlling the formation of landforms, but different area selection techniques are required to explore the local distribution of objects within subregions of higher population density that may be located inside the convex hull. In section 5.2 we use the convex hull method to explore regional patterns of spatial distribution among rootless eruption sites relative to a renormalized Poisson NN model, whereas in section 5.4.2 we consider the same NN model using an alternative area selection method. This alternative method uses ArcGIS to calculate A as the area of continuous domains with >10 rootless eruption sites per square kilometer. Values of A, ρ_0, and N are then used instead of A_{hull}, ρ_i, and N_i to calculate the properties of the expected NN distributions. Thus the convex hull method tests hypotheses regarding the regional distributions by assuming that the sample approximately represents a subset of an infinite domain, whereas the second method considers more local patterns of spatial organization by considering NN distributions within irregularly shaped domains of higher population density.

[52] We also compare the spatial distribution of rootless eruption sites in the Tartarus Colles region to those within the Hnúta and Hrossatungur groups of the 1783–1784 Laki lava flow in Iceland [*Hamilton et al.*, 2010a, 2010b]. *Hamilton*

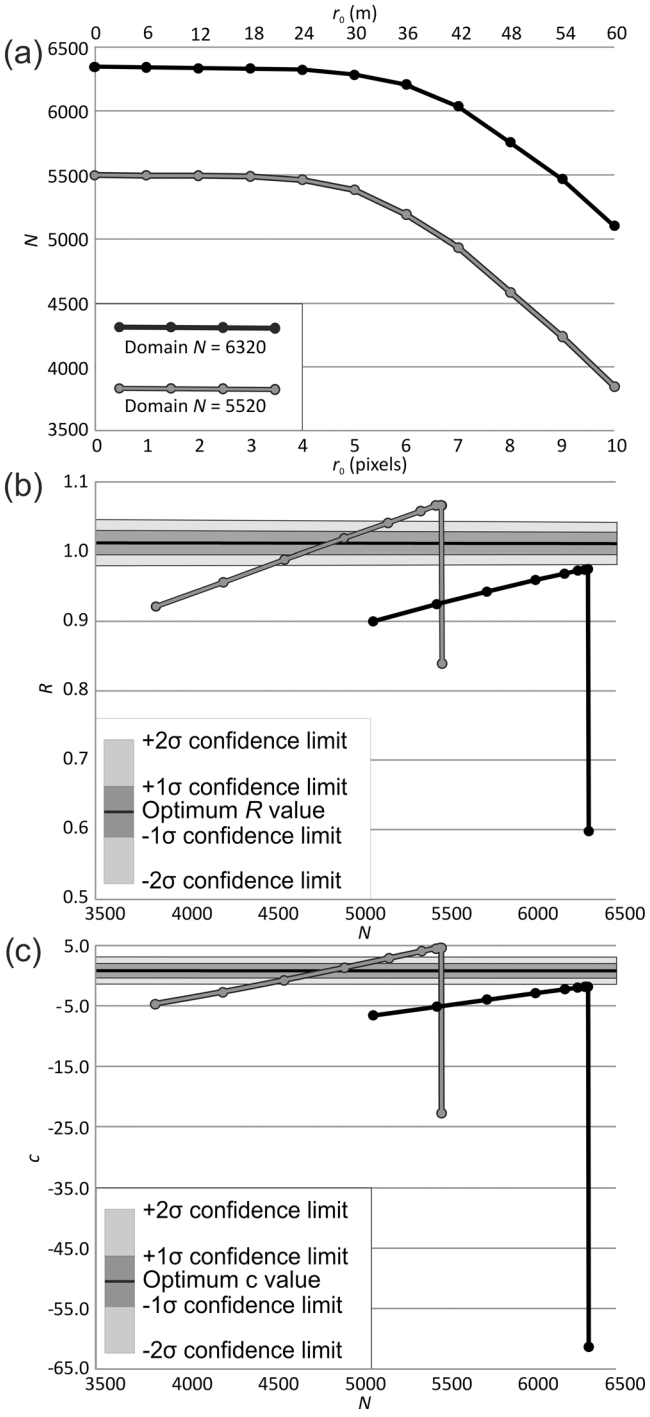

Figure 5. Effects of varying r_0 on renormalized Poisson nearest neighbor (NN) statistics. (a) Number of objects retained with the renormalization threshold r_0 increased in increments of 6 m (i.e., 1 CTX pixel). (b and c) NN statistics R and c, respectively, for each value of r_0. Changing r_0 from 0 to 1 CTX pixel results in significant changes in R and c, but R and c values remain stable for r_0 values ranging from 1 to 4 CTX pixels for the small domain (shaded) and 1 to 5 CTX pixels for the large domain (black). Further increases in r_0 result in significant variations in R and c as measured NN distances (r) fall below r_0.

et al. [2010b] used Poisson NN models, rather than renormalized Poisson distributions, when examining rootless eruption sites in the Hnúta and Hrossatungur groups of Iceland because their data set used Differential Global Positioning System (DGPS) measurements with sufficient accuracy and precision to resolve the smallest rootless eruption sites, which were 0.21 m in diameter. However, in this study, we must use the renormalized Poisson NN method of *Baloga et al.* [2007] because the locations of rootless eruption sites were determined using lower-resolution data (i.e., HiRISE and CTX imagery), which might not resolve the smallest surface expressions of rootless eruption sites and/or closest NN pairs. We do not present scavenged Poisson NN analysis results because many of the smaller VRC domains in the Tartarus Colles region contain an insufficient number of objects to be able to distinguish statistically between higher-order models [*Beggan and Hamilton*, 2010].

[53] To perform the renormalized Poisson NN analyses, the separation distance r between NN pairs is replaced by a term that accounts for a minimum detection threshold of distance r_0. This adjustment changes the standard Poisson NN distribution,

$$\rho(r) = 2\pi\rho_0 r e^{-\rho_0 \pi r^2}, \tag{5}$$

into the renormalized Poisson NN model [*Baloga et al.*, 2007],

$$\rho(r) = 2\pi\rho_0 r e^{\rho_0 \pi \left(r_0^2 - r^2\right)}. \tag{6}$$

Calculations of $\overline{r}_e$ and σ_e then become

$$\overline{r}_e = \frac{2\pi\rho_0}{e^{-\pi\rho_0 r_0^2}} \int_{r_0}^{\infty} r^2 e^{-\pi\rho_0 r^2} dr \tag{7}$$

$$\sigma_e = \sqrt{r_0^2 - r^2 + 1/\pi\rho_0}/\sqrt{N}. \tag{8}$$

[54] We set r_0 to the pixel size of the lowest-resolution satellite imagery used to digitize the location of rootless eruption sites, which in this case were CTX images with a resolution of 6 m/pixel. Although there are regions of higher-resolution data within our basemap mosaic (e.g., 25 cm/pixel HiRISE images), all input data were filtered to remove NN pairs separated by less than 6 m to ensure a uniform standard of comparison. A minimum detection threshold of one CTX pixel is a conservative value of r_0 because several pixels are typically required to identify a possible rootless eruption site and twice as many are required to distinguish a NN pair. However, we evaluate the sensitivity of our NN analyses to our choice of r_0 by performing the renormalized NN analysis on two domains within the Tartarus Colles region using r_0 values that range in increments of 6 m (i.e., 1 CTX pixel) from 0 m (equivalent to the standard Poisson NN model) to 60 m (Figure 5). The larger of these two test domains contains 6360 rootless eruption sites (N_i = 6344) and is located near the northernmost part of the western Tararus Colles volcanic unit (Figures 1 and 2), whereas the smaller domain (N = 5520, N_i = 5499) is located in the easternmost region of the study

area. The larger domain has a population density ρ_0 of 14.57 rootless eruption sites per square kilometer and a mean NN distance $\bar{r}_a$ of 113.2 ± 69.0 m (at 1σ), whereas the smaller domain has ρ_0 = 28.7 rootless eruption sites per square kilometer and $\bar{r}_a$ = 84.9 ± 43.6 m.

[55] Figure 5a shows that increasing r_0 from 0 to 6 m results in minimal loss of data (<0.1%) in both the larger (black) and smaller (shaded) domains because few NN pairs have a separation distance r that is below r_0. Nonetheless, the introduction of a renormalization threshold substantially changes R (Figure 5b) and c (Figure 5c). For instance, introducing a threshold of r_0 = 6 m increases R from 0.60 to 0.98 for the larger domain and from 0.84 to 1.07 for the smaller domain. Similarly, c changes from −61.24 to −1.83 and from −22.78 to 4.61 for the larger and smaller domains, respectively. For r_0 = 0 and 6 m, the larger domain shows statistically significant tendencies toward clustering with R and c being outside their respective 2σ confidence intervals. In contrast, the smaller domain shows statistically significant departures from the null hypotheses with R and c outside their 2σ confidence limits. However, relative to the standard Poisson model (with r_0 = 0), the R value is less than the lower bound of its 2σ confidence interval, and, relative to the renormalized Poisson model (with r_0 = 6 m), R is greater than its upper 2σ confidence limit. Thus increasing r_0 from 0 to 6 m causes a dramatic change in the apparent spatial distribution of rootless eruption sites in the smaller domain, with the results implying clustering relative to the standard Poisson model and repelling relative to the renormalized Poisson model.

[56] Further increasing the renormalization threshold causes R and c to decrease monotonically as more data are discarded from the input distribution once r falls below r_0. For instance, within the larger domain, 2.1% of the data are lost when r_0 is increased from 6 to 36 m (i.e., from 1 to 6 CTX pixels). Over the same range of r_0, R decreases from 0.98 to 0.97 and c decreases from −1.83 and −2.26. For the smaller domain, 2.2% of the data are lost when r_0 is increased from 6 to 30 m (i.e., 1 to 5 CTX pixels). Correspondingly, R decreases from 1.07 to 1.06 and c decreases from 4.6 to 4.0. Within these ranges of r_0, both domains continue to show significant departures from the null hypothesis, with rootless eruption sites tending toward clustering in the larger domain and toward repelling in the smaller domain. However, further increasing r_0 by 6 m (i.e., 1 CTX pixel) more than doubles the amount of data that are lost in both domains and generates substantially lower R values. For the larger domain this results in a stronger tendency toward clustering, whereas for the smaller domain, R and c move to within their 2σ confidence intervals, thereby implying that for some choices of r_0, the spatial organization of the rootless eruption sites in the smaller domain can be described by the null hypothesis. An additional increase in r_0 to 54 m (i.e., 9 CTX pixels) causes 23% of the data in the smaller domain to be discarded. Accordingly, R and c decrease to the point where the rootless eruption sites appear to exhibit statistically significant clustering relative to the null hypothesis, but with nearly a quarter of the data being excluded, this analysis fails to be representative of the original distribution.

[57] These examples demonstrate that relative to a standard Poisson NN analysis, the introduction of a renormalization threshold can significantly affect NN results by causing substantial variations in R and c. Thus it is important to choose a value of r_0 that accurately reflects data resolution limitations, without adopting a value that is so large as to bias the NN results by discarding an excessive amount of data and forcing R and c to become erroneously low. In this study, we apply a conservative threshold of r_0 = 1 CTX pixel (i.e., 6 m) because NN statistics generated with this r_0 value retain >99.9% of the original data and yet are representative of results generated over a broader range of r_0, which includes choices of r_0 of 5–6 CTX pixels. In other applications, it may be preferable to specify r_0 >1 pixel, but in all cases we recommend that analysts explore the effects of changing r_0 in their particular application, especially in instances where renormalized NN results are very close to the limits of significance for R and c.

5.2. NN Analysis of Rootless Eruption Sites

[58] Table 1 summarizes NN analysis results for the 36 VRC domains in the Tartarus Colles region with ≥30 rootless eruption sites. These results evaluate the null hypothesis that the spatial distribution of rootless eruption sites in each domain is consistent with a renormalized Poisson distribution given sample-size-dependent thresholds of significance for R and c. All of the NN statistics presented in Table 1 are calculated using convex hull areas (A_{hull}) and r_0 = 6 m. Table 1 shows the total number of objects in each domain (N), the total number of objects located inside each convex hull (N_i), A_{hull}, and A, which is the domain area as defined by a continuous region with a population density >10 rootless eruption sites per square kilometer. For each domain, Table 1 also presents the mean measured NN distance ($\bar{r}_a$), its standard deviation (σ), standard error (σ_e), range, skewness, and kurtosis. Skewness and kurtosis values presented in this study and by *Hamilton et al.* [2010b] were calculated using GIAS version 1.12, which implements MATLAB's standard statistical functions. These functions include skewness and kurtosis definitions that differ from those used by *Baloga et al.* [2007] as well as some statistical programs and spreadsheets such as Microsoft Excel (see GIAS help files for more detail, available at www.geoanalysis.org). Thus, for those interested in comparing NN statistics presented in different studies, we caution that differences in underlying methodologies must be carefully considered because they can produce systematic differences in NN results such as skewness and kurtosis values.

[59] Table 1 also evaluates the significance of R and c relative to 1 and 2σ confidence internals. If R is within ±1σ thresholds of significance for the ideal value of R given a particular sample population size, Table 1 expresses the "confidence in R" as <1σ, whereas if R outside the 1σ confidence interval but within ±2σ, then the confidence in R is presented as <2σ. Similarly, if R is outside of the ±2σ confidence interval, confidence in R is >2σ. The same notation applies to the "confidence in c." Using ±2σ limits of uncertainty to define thresholds of significance for both R and c, the rightmost column of Table 1 summarizes the implication of R and evaluates its significance. Within this framework, R can have one of three implications: "random," meaning that R is within its 2σ confidence interval (i.e., the 0.95 confidence interval) and thus is approximately equal to the ideal value of R that would be expected for a

Table 1. Renormalized Poisson Nearest Neighbor (NN) Analysis Results (r_0 = 6 m; A_{hull})

N	N_i	A (km^2)	A_{hull} (km^2)	r_a (m)	1σ (m)	1σ_e (m)	Range of r_a (m)	Skewness	Kurtosis	R	c	Confidence in R	Confidence in c	Implication (Significant)
15,687	15,665	1,117.21	2,190.40	108.8	108.8	0.9	5.0–701.7	1.74	7.72	0.95	−5.92	>2σ	>2σ	clustered (yes)
6,360	6,340	436.38	909.35	113.2	69.0	0.9	3.7–652.8	2.04	9.67	0.98	−1.83	>2σ	>2σ	clustered (yes)
5,520	5,497	192.11	224.99	84.9	43.6	0.6	3.5–589.2	2.23	14.23	1.07	4.61	>2σ	>2σ	repelled (yes)
3,680	3,658	221.73	423.79	101.1	60.3	1.0	15.1–652.2	2.34	13.82	0.97	−1.90	>2σ	>2σ	clustered (yes)
3,279	3,260	142.28	214.35	71.8	56.6	1.0	10.2–649.4	2.83	16.29	0.97	−1.55	>2σ	>2σ	clustered (yes)
1,183	1,175	55.25	73.48	84.7	45.0	1.3	24.4–395.5	1.74	7.82	1.01	0.22	<1σ	<1σ	random (yes)
989	974	58.06	64.19	93.3	54.7	1.8	18.9–383.0	1.69	6.93	1.04	1.00	<1σ	<1σ	random (yes)
613	598	49.86	59.72	115.1	72.9	3.0	27.7–566.6	2.04	9.06	1.06	1.22	<2σ	<1σ	random (yes)
390	376	36.68	45.08	121.1	75.7	3.9	20.0–507.9	1.91	8.64	1.02	0.27	<1σ	<1σ	random (yes)
322	312	25.47	20.86	119.6	63.8	3.6	37.1–496.1	1.63	7.64	1.11	1.85	>2σ	<1σ	repelled (no)
244	235	13.05	8.27	90.2	43.3	2.8	25.5–390.9	2.23	12.95	1.11	1.54	>2σ	<1σ	repelled (no)
233	223	22.20	20.53	109.6	65.8	109.6	19.8–441.1	1.35	6.01	1.00	0.00	<1σ	<1σ	random (yes)
204	193	14.35	11.39	90.9	50.3	3.6	29.9–336.7	1.90	8.21	1.05	0.62	<1σ	<1σ	random (yes)
165	156	12.24	10.62	104.5	64.1	5.1	30.8–458.9	1.95	9.31	1.07	0.76	<1σ	<1σ	random (yes)
156	145	12.38	10.47	113.2	59.9	4.9	1.2–380.6	1.60	7.13	1.07	0.74	<1σ	<1σ	random (yes)
139	127	12.12	8.94	129.4	74.4	6.6	28.3–447.9	1.40	5.91	1.15	1.56	>2σ	<1σ	repelled (no)
130	121	13.06	11.23	116.6	76.9	7.0	27.4–487.8	1.88	7.87	1.07	0.68	<1σ	<1σ	random (yes)
99	89	8.02	5.56	106.5	61.9	6.6	35.0–328.8	1.50	5.50	1.11	0.94	<1σ	<1σ	random (yes)
98	88	10.98	9.87	149.6	87.0	9.3	29.0–542.3	2.31	10.15	1.12	1.03	<2σ	<1σ	random (yes)
91	79	6.26	3.26	85.5	45.4	5.1	25.5–249.5	1.60	5.89	1.09	0.76	<1σ	<1σ	random (yes)
85	75	7.82	5.22	104.8	60.0	6.9	27.6–288.3	1.03	3.77	1.05	0.36	<1σ	<1σ	random (yes)
84	71	6.49	4.46	4.1	208.1	24.4	4.1–208.1	0.38	2.40	12.89	0.11	<1σ	<1σ	random (yes)
64	55	6.72	5.43	126.4	94.2	12.7	46.1–469.4	2.05	7.01	1.18	1.21	<2σ	<1σ	random (yes)
50	43	5.25	3.06	124.7	75.3	11.5	49.0–344.4	1.50	4.70	1.20	1.18	<2σ	<1σ	random (yes)
48	41	5.09	2.82	72.6	73.5	11.5	18.9–452.8	3.80	19.29	1.07	0.38	<1σ	<1σ	random (yes)
48	39	4.25	1.70	77.1	63.4	10.2	27.7–375.8	3.22	14.57	1.16	0.91	<1σ	<1σ	random (yes)
43	34	4.71	2.12	137.7	128.4	22.0	57.6–646.2	3.37	13.34	1.31	1.75	>2σ	<1σ	random (yes)
43	33	8.96	7.55	246.9	171.9	29.9	79.5–965.8	2.59	10.74	1.23	1.25	<2σ	<1σ	random (yes)
40	32	2.71	1.06	97.5	61.1	10.8	37.0–302.1	1.86	6.65	1.22	1.17	<2σ	<1σ	random (yes)
37	28	3.63	1.33	119.0	69.3	13.1	51.7–290.4	1.07	3.14	1.29	1.41	<2σ	<1σ	random (yes)
37	30	4.21	2.19	135.2	12.9	2.4	24.8–259.3	0.54	2.41	0.87	−1.33	<2σ	<2σ	random (yes)
69	59	5.34	4.08	131.5	8.9	1.2	47.1–415.5	1.78	6.79	1.17	1.17	<2σ	<1σ	random (yes)
34	26	2.71	0.73	98.7	41.9	1.7	32.3–193.9	0.35	2.70	1.15	0.70	<1σ	<1σ	random (yes)
32	24	2.73	0.98	126.4	49.9	10.2	45.5–218.7	0.07	1.98	1.18	0.81	<1σ	<1σ	random (yes)
31	23	3.94	2.66	155.5	136.6	28.5	53.7–505.5	1.57	4.27	1.43	1.79	>2σ	<1σ	repelled (no)
31	23	2.85	1.68	124.0	48.9	10.2	55.9–211.4	0.31	2.14	1.04	0.20	<1σ	<1σ	random (yes)

renormalized Poisson distribution of equivalent population size; "repelled," indicating that the null hypothesis is not supported with 2σ confidence limits in R because $\bar{r}_a$ is substantially greater than $\bar{r}_e$; or "clustered," suggesting that R does not support the null hypothesis within $\pm 2\sigma$ limits because $\bar{r}_a$ is considerably less than $\bar{r}_e$. The significance of these implications is evaluated using c. For instance, "repelled (yes)" and "clustered (yes)" mean that the value of R implies a departure from the null hypothesis that either tends toward repelling (if $\bar{r}_a > \bar{r}_e$ and R is above its upper 2σ threshold) or clustering (if $\bar{r}_a < \bar{r}_e$ and R is below its lower 2σ threshold), and these results are significant because c is also outside its 2σ confidence interval. Alternatively, if R is outside its 2σ confidence interval but c is within its $\pm 2\sigma$ thresholds, then the implied repelling or clustering is not significant and this result would be expressed in Table 1 as "repelled (no)" or "clustered (no)." In Table 1, "random (yes)" indicates that the result of R implies that the input distribution is described by the null hypothesis and that this implication is significant because both R and c are within their $\pm 2\sigma$ thresholds. A situation where R is within its 2σ confidence interval but c is outside its $\pm 2\sigma$ threshold would indicate an inconclusive result because R would imply that the null hypothesis describes the spatial distribution of the data, while c indicates that the results implied by R are not significant. However, this situation does not occur within the Tartarus Colles region.

[60] Figures 6a and 6b present plots of R and c values versus $\log(N_i)$ for each of the Tartarus Colles domains as well as for the Hnúta and Hrossatungur groups [*Hamilton et al.*, 2010b]. On Earth and Mars, rootless eruption sites tend to be randomly distributed within small domains, with clustering tending to increase as the number of objects increases (Figures 6a and 6b). In some cases, repelling beyond the 2σ confidence interval for R was observed within small domains in the Hnúta and Hrossatungur groups [*Hamilton et al.*, 2010b], but within the Tartarus Colles region only one domain (N = 5520) shows a statistically significant tendency toward repelling relative to the renormalized Poisson model. Five smaller domains in the Tartarus Colles region, with N ranging from 31 to 322, exhibit tendencies toward repelling, but these results are not significant within the 2σ confidence interval of c. All other domains with $N <$ 3279 were consistent with the renormalized Poisson model. For $N \geq 3279$, four of the five domains showed statistically significant departures from the null hypothesis with tendencies toward clustering. Thus within the Tartarus Colles region, rootless eruptions sites appear to be randomly distributed in 26 of 36 domains. However, there is an increased tendency toward clustering within domains that include $\gtrsim$3000 rootless eruption sites. These relationships hold true not only for population size, but also for domain area because the number of objects in each domain (N) is strongly correlated with domain area.

5.3. Geospatial Analysis: Lava Thickness Relationships

[61] The thickness of the Tartarus Colles lava flow north of 26°N is estimated by subtracting an inclined plane with a constant slope of 0.05° from MOLA 128°/pixel MEGDR elevation data (Figure 7). This approach assumes that the smooth plains unit projects beneath the Tartarus Colles volcanic unit and that there are no dramatic changes in topography beneath the lava. South of 26°N, the Tartarus Colles lava flow moved through valleys incised into the high-standing Nepenthes Mensae unit, and therefore a smooth underlying topography cannot be reasonably assumed in this region. For this reason, we restrict our lava thickness estimates to the northern part of flow, which is adjacent to the smooth plains unit (see inset location in Figure 2). Nonetheless, we caution that even though the gently sloping smooth plains unit appears to underlie the Tartarus Colles lava flow north of 26°N, hidden variations in underlying topography could affect our lava thickness estimates.

[62] Figure 8 shows lava thickness frequencies binned to 5 m intervals. The histogram for the Tartarus Colles lava flow (Figure 8a) shows that the lava exhibits a bimodal thickness with peaks at 25–30 m and 55–60 m. The presence of rootless tephra on the surface of the Tartarus Colles lava flow may locally increase the apparent thickness of the flow, but the bimodality of the lava thickness distributions (Figure 8a) strongly implies that the Tartarus Colles lava flow is composed of two plateaus, one with a thickness of 25–30 m and the other of 55–60 m. Additionally, we observe that lava thicknesses >75 m constitute only 2.1% of the Tartarus Colles lava flow. Lava flow thicknesses associated with rootless eruption sites exhibit a unimodal distribution with a mean of 58.4 m ($\pm 1\sigma$ = 8.2 m, $\pm 1\sigma_e < 0.1$ m, N = 29,654). Only 0.27% of the total number of rootless eruption sites (i.e., 81 of 29,652) occur where the lava is <30 m thick. In contrast, lava thicknesses associated with the pitted terrains (Figure 8c) exhibit a bimodal distribution with peaks at 35–40 m and 60–65 m. These results demonstrate that rootless eruption sites preferentially concentrate within the thicker lava plateau, whereas pitted terrains occur throughout both plateaus of the Tartarus Colles lava flow.

5.4. Geospatial Analysis: Discussion

5.4.1. Patterns of Spatial Distribution for Landforms Within the Tartarus Colles Region

[63] Over increasingly large areas the NN distances between rootless eruption sites in the Tartarus Colles region tend to exhibit increasingly significant departures from the renormalized Poisson NN model (r_0 = 6 m), with R values implying a tendency toward clustering. This suggests that over regional scales, the resources required to generate rootless eruptions (i.e., lava and water) were heterogeneously distributed at the time of VRC formation [*Baloga et al.*, 2007; *Hamilton et al.*, 2010b]. Similar patterns were observed within the Hnúta and Hrossatungur groups and interpreted as the result of preeruption topography, which concentrated both near-surface water and lava into paleotopographic lows [*Hamilton et al.*, 2010b]. The majority of VRCs in the western Tartarus Colles region are located north of where lava emerged from a valley system [*Hamilton et al.*, 2010c]. Thus, while topography may have exerted an important control on the distribution of rootless eruption sites within the valley network, topography alone does not explain the clustering of rootless eruption sites where the lava was largely unconfined by paleotopography north of ~26°N.

[64] The preferential occurrence of rootless eruption sites within the thicker (~60 m) parts of the Tartarus Colles lava flow strongly implies that flow thickness was a critical factor in determining the location of rootless eruptions. *Hamilton*

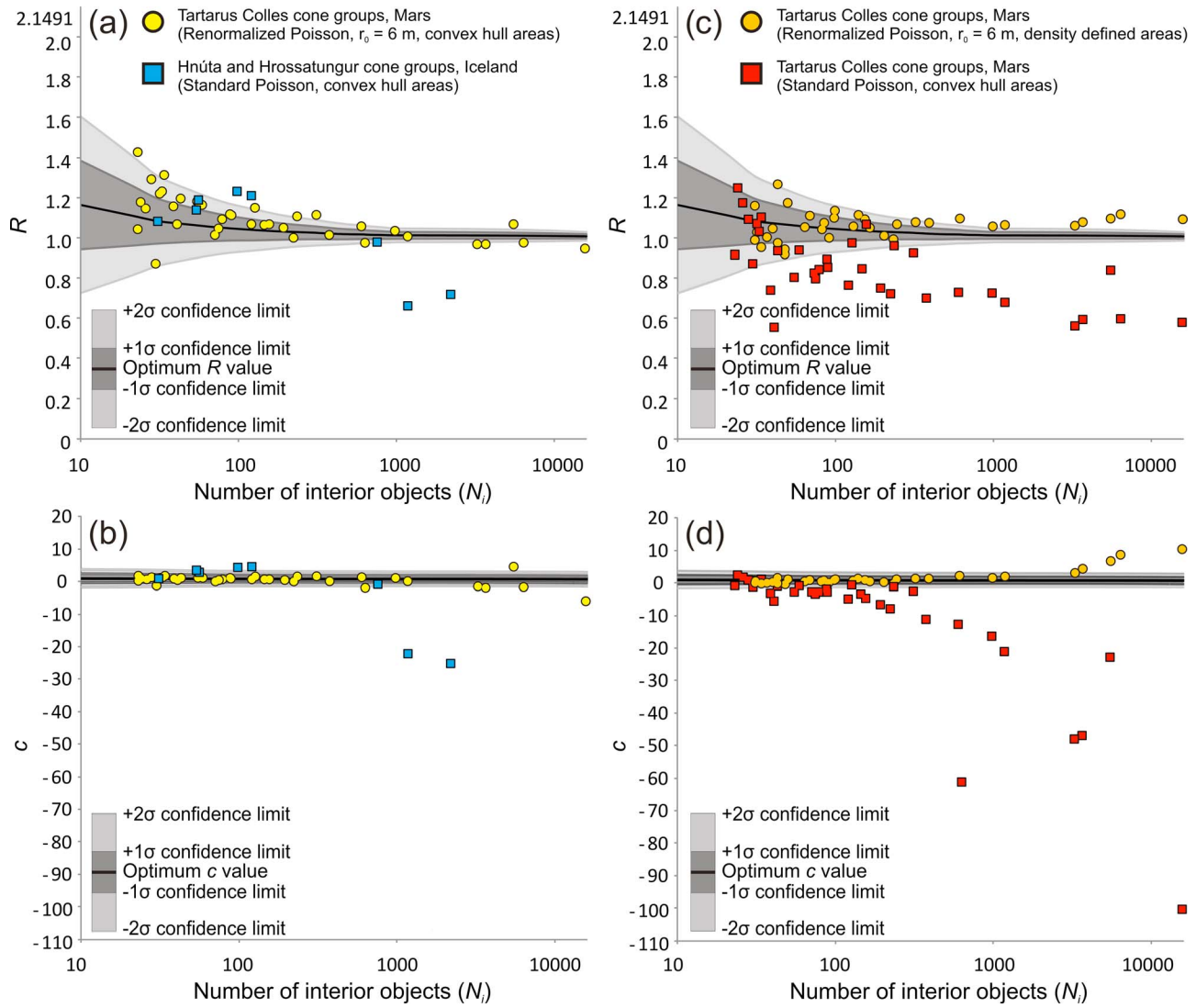

Figure 6. NN analysis results. (a) *R* values for VRC domains in the western Tartarus Colles region of Mars (yellow) obtained using a renormalized Poisson NN method (r_0 = 6 m). Also shown are *R* values for domains in the Hnúta and Hrossatungur groups of Iceland (blue) obtained using a standard Poisson NN method. The maximum *R* value of 2.1491 corresponds to a perfectly uniform distribution [*Clark and Evans*, 1954]. (b) Corresponding *c* values for each domain are shown in Figure 6a. On Mars and in Iceland, rootless eruption sites exhibit similar scale-dependent variations in spatial organization with *R* generally decreasing with increasing population size. (c) *R* values for VRC domains in the western Tartarus Colles region (red) using the standard Poisson NN analysis method. These results show greater clustering relative to the renormalized Poisson method. In contrast to the other NN analyses, which utilize convex hull areas, results in orange are based on renormalized Poisson NN analysis of rootless eruption sites in the western Tartarus Colles region using density domain areas (specified using a threshold of 10 rootless eruption sites per square kilometer) instead of convex hull areas. These results show a significant increase in *R*. (d) *c* values for the domains shown in Figure 6b. Yellow points shown in Figures 6a and 6b correspond to the entries in Table 1.

et al. [2010c] inferred that only the thicker parts of the lava flow delivered enough heat into the substrate to vaporize H_2O within a ground ice reservoir before the lava became too viscous to produce rootless eruptions through MFCIs. Our results support this interpretation and provide additional evidence to suggest that the spatial distribution of rootless eruptions was controlled largely by the location of preferred lava pathways that inflated to ~60 m thickness. This made the thicker portions of the Tartarus Colles lava flow more favorable environments for generating rootless eruptions than the peripheral regions of the flow, which stagnated at ~30 m thickness, because the thicker lava plateau had a greater through flux of lava, was active for a longer period of time, and was able to melt more of the underlying ground ice before the core of the flow solidified.

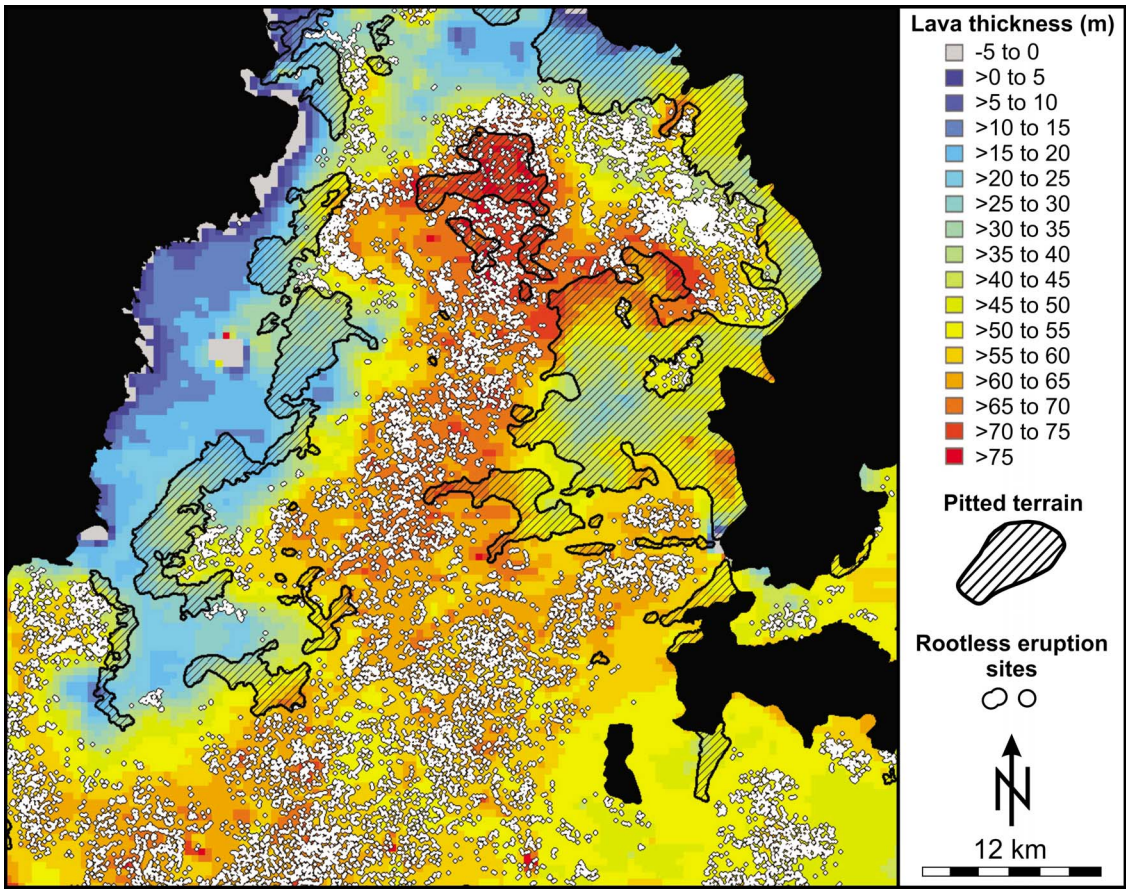

Figure 7. Estimated thickness of the Tartarus Colles lava flow based on an elevation residual obtained by subtracting an inclined plane with a constant slope of 0.05° from 128°/pixel Mars Orbiter Laser Altimeter (MOLA) Mission Experiment Gridded Data Record (MEGDR) elevation data. This figure corresponds to the Figure 2 inset, which spans from 27°N, 170.2°E (upper left corner) to 26°N, 171.2°E (lower right corner). Pitted terrains are represented by diagonally hatched regions, whereas rootless eruption sites are individually marked by white dots.

5.4.2. Regional Clustering and the Effects of Area Selection on NN Statistics

[65] Analyzing the NN distances of objects within convex hull boundaries is useful for quantifying the heterogeneity of object distributions. However, if objects are not distributed throughout the whole convex hull region, NN results can be biased toward clustering. For instance, by using the convex hull method, we replace population density ($\rho_0 = N/A$) with the population density inside the convex hull ($\rho_i = N_i/A_{\text{hull}}$). Typically, $N_i \approx N$, but if the geometry of the feature field exhibits significant embayment, then A_{hull} can deviate substantially from A (Figures 9a and 9b). In Figure 9c we plot the ratio A_{hull}:A versus N. For population sizes $\lesssim$350 this ratio is <1, indicating that A_{hull} is smaller than the corresponding density threshold domain area (A). In contrast, for $N \gtrsim 350$, A_{hull} exceeds A. This is understandable given that our density calculations use 100 m wide cells with a search radius of ~0.5 km because this method smoothes the domain boundaries by adding a 5 pixel wide buffer around rootless eruption sites. This buffer coincides very well with the extent of the platform facies associated with the VRC domains, but it can make A larger than A_{hull} for domains that lack significant embayment. Differences between A_{hull} and A can be useful for quantifying the degree of regional clustering, but it is important to remember that if objects are heterogeneously distributed, regional NN statistics do not necessarily provide an accurate portrayal of the patterns of spatial distribution within embedded areas of interest. Thus, as domain embayment become significant, A_{hull} will exceed A, which in turn will decrease ρ_i relative to ρ_0, increase $\bar{r}_e$, and decrease R because $R = \bar{r}_a/\bar{r}_e$ (equation (3)). Low R values therefore indicate that objects are clustered relative to a Poisson model applied throughout the whole convex hull region. In Figure 6a, low R values are interpreted as being indicative of regional clustering of rootless eruption sites, but to understand the patterns of spatial organization within the embedded regions of higher VRC density, we must consider the distribution of rootless eruption sites within A rather than A_{hull}.

[66] Using A_{hull} to define domain areas, the only regions of interests that exhibit statistically significant clustering are those with $N \gtrsim 3000$ (Figure 6). In contrast, rootless eruption sites in domains with $N \lesssim 3000$ tend to be randomly distributed. However, by reanalyzing the NN distributions of the domains using areas that are defined by the regions covered by >10 rootless eruption sites per square kilometer (i.e., A), rather than A_{hull}, our results show that none of the

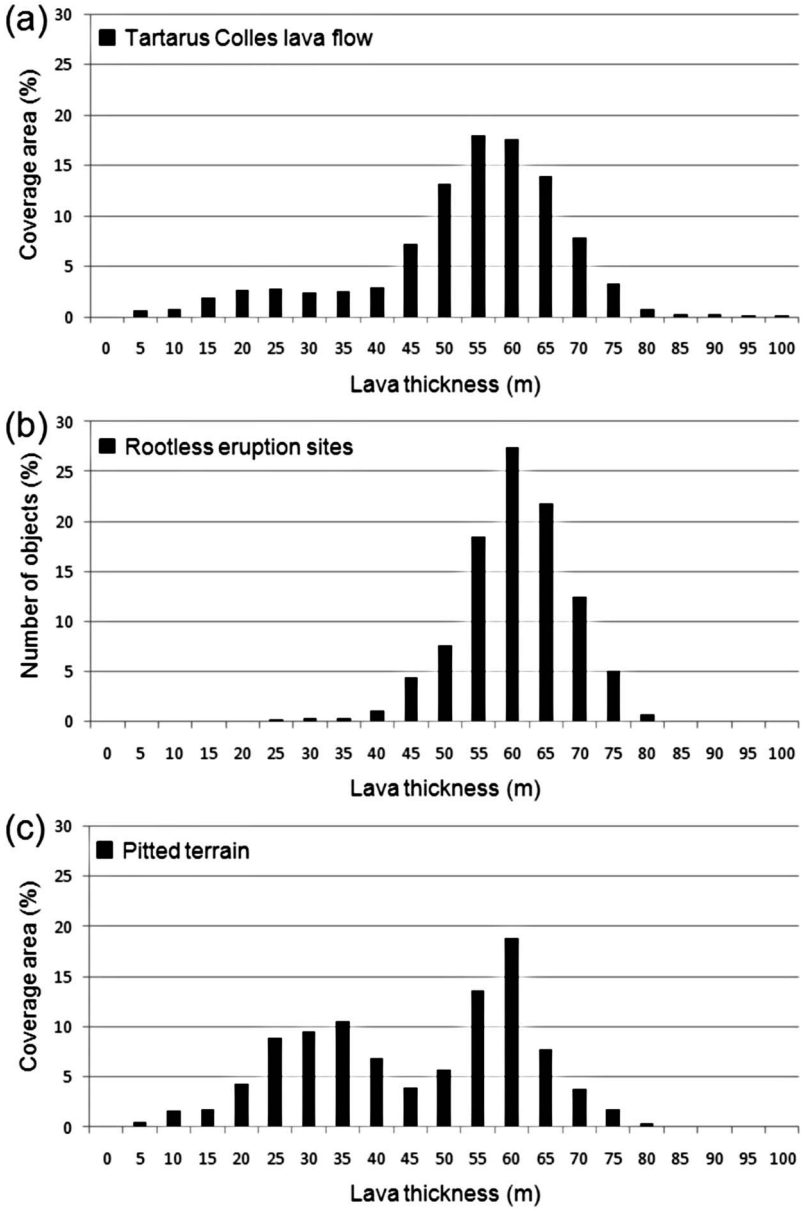

Figure 8. (a) Lava thickness distribution within the Tartarus Colles lava flow. (b) Thickness of the Tartarus Colles lava at rootless eruption sites. (c) Thickness of the Tartarus Colles lava flow within pitted terrain regions.

domains maintain statistically significant clustering beyond the 2σ limits for R and c (Figures 6c and 6d). Instead all five of the largest domains (N = 3279 to 15,687) exhibit statistically significant departures from the renormalized Poisson model (r_0 = 6 m), with tendencies toward repelling. On the basis of the values of R, the four next largest domains ($N >$ 390) also show tendencies toward repelling, but the c values indicate that the results are not significant beyond 2σ confidence limits. The spatial distribution of rootless eruption sites in all but one of the remaining domains (27 of all 36 domains) are consistent with the renormalized Poisson model (r_0 = 6 m). The only exception (N = 43) shows a tendency toward repelling, but the results are not significant within the 2σ confidence interval of c. From these results we conclude that even when differences between A_{hull} and A are considered, rootless eruption sites generally appear to form at random locations within parts of the Tartarus Colles lava flow that are ~60 m thick. However, we observe that over large regions, domains that are favorable for the formation of VRCs are irregularly shaped in plan view and can exhibit pronounced embayment relative to their corresponding convex hull regions. These large, irregularly shaped VRC domains are also crosscut by pitted terrains (Figures 1 and 7) and show evidence of being dissected through a post-emplacement modification process (Figures 3j–3l). When these embayed domain geometries are accounted for by substituting A for A_{hull}, NN in domains with $N \gtrsim 3000$ appear to be repelled relative to the renormalized Poisson model (r_0 = 6 m). This could mean that the formation of rootless eruption sites in the largest domains was controlled by a

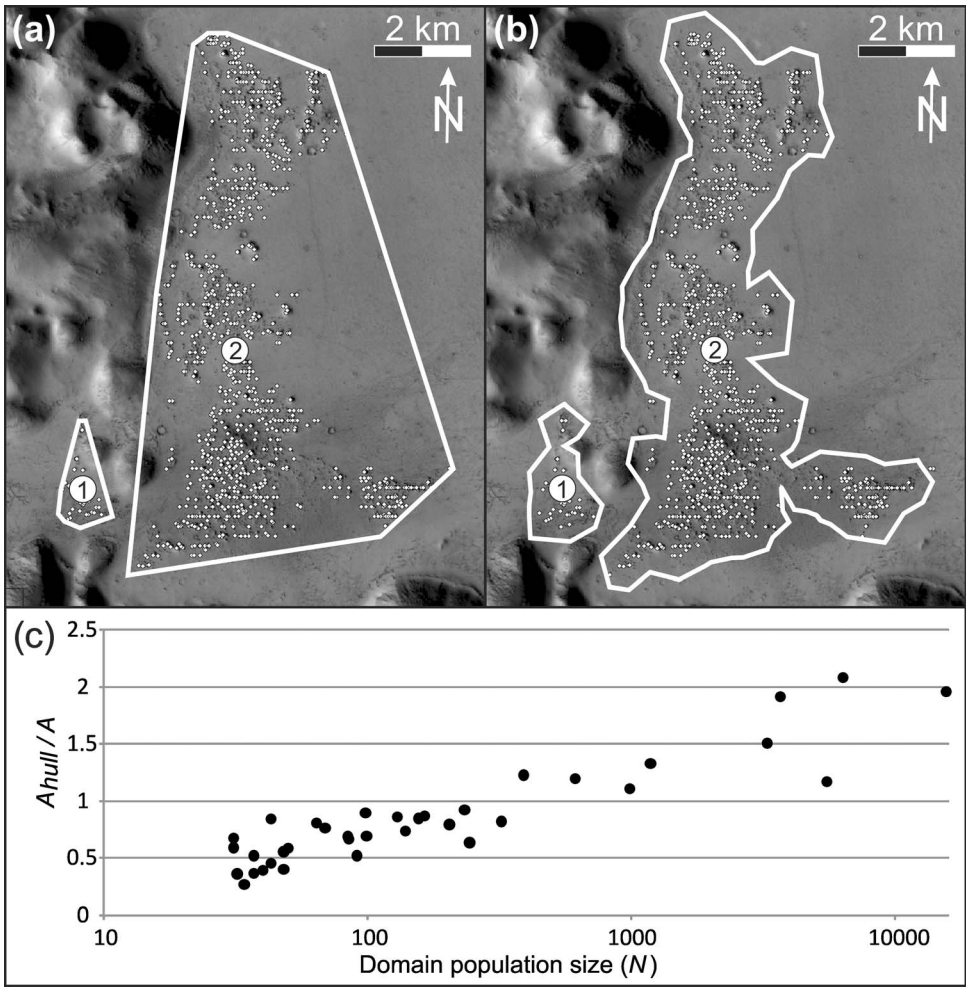

Figure 9. Example of VRC-covered domains embedded within convex hull regions. (a) Convex hull boundaries surrounding two VRC domains with rootless eruption sites identified by white dots. Rootless eruption sites in Figures 9a and 9b appear to exhibit horizontal lineations, but these are artifacts of ArcGIS rendering and are not present within the data at higher magnifications. The depicted region spans from 25.7°N, 171.2°E (upper left corner) to 25.4°N, 171.4°E (lower right corner). Domain 1 has $N = 34$, and domain 2 has $N = 989$. (b) Population density boundaries for the same region with a threshold of >10 rootless eruption sites per square kilometer. Typically, $N_i \approx N$, but if the geometry of the feature field exhibits significant embayment, then A_{hull} can deviate substantially from A. For instance, in Figures 9a and 9b, the smaller of the two domains (labeled 1) has a convex hull area (A_{hull}) that is less than the population density area A, whereas for the larger domain (labeled 2), $A_{\text{hull}} > A$. (c) Ratio of the convex hull area (A_{hull}) to the density threshold-defined (>10 rootless eruption sites/km^2) domain area A versus the population size N within the domain for domains with $N > 30$.

nonrandom process that differed from the random formation of rootless eruptions in the smaller domains. However, on the basis of geomorphological evidence, we interpret the apparently repelled distributions in the largest domains to be a consequence of the pitted terrains, which formed after the rootless eruption sites and destroyed parts of their initially random distribution. Observed differences between the geospatial organization of rootless eruption sites in domains of different sizes may therefore result from differences in VRC preservation, rather than differences in their modes of formation.

5.4.3. Comparison With Previous Studies

[67] Within the western Tartarus Colles region, rootless eruption sites in most VRC domains have spatial distributions that are consistent with a renormalized Poisson NN model ($r_0 = 6$ m). The conclusion that the rootless eruption sites dominantly exhibit random distributions is consistent with the results of *Bishop* [2008], but we caution that *Bishop* [2008] only examined the spatial distribution of landforms within MOC imagery and these image swaths do not contain natural boundaries for the VRC domains.

[68] Using continuous CTX mosaics to define the locations of rootless eruption sites, we are able to perform NN analyses using both convex hull areas (A_{hull}) and natural domain boundaries (A). The only significant difference that occurs when using A in place of A_{hull} is that the apparent distribution of rootless eruption sites within the largest domains changes from being clustered to being repelled.

This is understandable given that the irregular shape of the largest VRC domains results in rootless eruption sites being clustered within a subset of the convex hull region. However, even when this effect is corrected for by using A instead of A_{hull}, the NN distributions for rootless eruption sites in the largest domains are not well described by the null hypotheses of spatial randomness. Instead, they appear repelled relative to a random distribution. Given the morphological similarity of VRCs in domains of all sizes, we assume that their initial distributions may also have been similar. However, the co-occurrence of pitted terrains in the largest domains suggests that repelling may have been caused by the formation of the pitted terrains, which destroyed some members of an originally random distribution to leave surviving members of the population with greater than random NN distances. If this is the case, then the mechanism for generating repelling at regional scales within in the Tartarus Colles cone groups varies substantially from the repelling caused by local self-organization processes in Iceland.

[69] Within the Hnúta and Hrossatungur groups of Iceland, rootless eruption sites cluster in spaces between topographic highs but exhibit a tendency toward locally repelled spatial distributions [*Hamilton et al.*, 2010a, 2010b]. *Hamilton et al.* [2010b] concluded that VRCs preferentially form in regions of low elevation that concentrate near-surface water and the flow of lava, but rootless eruption sites can locally self organize into distributions reflecting the noninitiation and/or early cessation of rootless eruptions at locations with insufficient access to groundwater.

[70] Repelling has also been documented among VRCs in the western Tartarus Colles region [*Baloga et al.*, 2007]. However, after reanalyzing the same region using HiRISE data instead of MOC imagery, we determined that the rootless eruption sites have a slight tendency toward greater than random NN spacing (R = 1.08, which is above the upper 2σ limit of 1.05), but that the result is not statistically significant (c = 1.41, which is within the 1σ limits of −0.28 to 1.84). Our observation of weaker tendency toward repelling may in part be due to object selection methodology. In our approach, VRCs are parsed into constituent rootless eruption sites, whereas *Baloga et al.* [2007] considered VRCs are undivided structures. Consequently, the mean NN distance in our input distribution ($\bar{r}_a$) would be smaller than that of *Baloga et al.* [2007], which in turn would lead to lower R values and a decreased tendency toward repelling.

[71] In contrast to *Bruno et al.* [2004, 2006] and *Burr et al.* [2009a], our NN analyses indicate that rootless eruption sites do not invariably cluster relative to a Poisson random model. This is due primarily to differences between our renormalized Poisson NN technique and their standard Poisson NN methodology. In Figure 5, we showed that by defining $r_0 > 0$, NN statistics can exhibit reduced tendencies toward clustering and, in some instances, even appear repelled. Running our analyses using a standard Poisson NN analysis method (Figures 6c and 6d) results in 23 of the 36 input distributions deviating from the null hypothesis by more than the 2σ confidence intervals for R and c, with each of the 23 nonrandom distributions tending toward clustering. The remaining 13 domains are randomly distributed within 2σ confidence limits (Figures 6c and 6d). However, given the resolution limits of our data, we consider NN analyses that use the renormalized Poisson model to be more reliable. Consequently, the strong tendency toward clustering among VRCs that has been previously documented among possible rootless eruption sites on Mars [e.g., *Bruno et al.*, 2004, 2006; *Burr et al.*, 2009a] may be an artifact of overlooking data resolution limitations.

[72] In summary, our analyses show that there is no single NN statistic that is diagnostic of VRC identity. Relative to standard Poisson and renormalized Poisson models, the geospatial distributions of rootless eruption sites in the western Tartarus Colles region are typically random but can range from repelled to clustered. This result generally agrees with *Bishop* [2008], in that he concluded that the Tartarus Colles cone groups are composed of landforms that dominantly have random distributions. However, we have also observed that among the largest domains ($N \gtrsim 3000$), NN statistics are strongly influenced by VRC domain geometry because rootless eruption sites are not homogeneously distributed throughout all of the convex hull regions. This can introduce a tendency toward clustering when A_{hull} is used to define the area of the feature field, but when convex hull effects are accounted for by substituting A for A_{hull}, we observe that the largest domains tend to be repelled. We attribute this result to a postemplacement modification process, which may have destroyed some members of an originally random population to generate greater than random NN distances between the surviving rootless eruption sites. However, it possible that the original distributions of VRCs within the largest domains were systematically different from those within the smaller domains for some other reason, such as a difference in the underlying topography, initial ground ice distribution, and/or lava emplacement processes.

6. Paleoenvironmental Interpretation

6.1. Formation of the Tartarus Colles Cone Groups and Pitted Terrains

[73] Figure 10 summarizes our interpretation of the formation of the Tartarus Colles volcanic unit. The morphologies and spatial distributions of the putative VRCs within this unit suggest that these landforms are the products of explosive lava-water interactions. The presence of elongated VRCs and radially symmetric cratered cones within the same lava flow also provides evidence that the explosive lava-water interactions occurred over an extended period of time, with rootless eruptions initiating while the lava flow surface was in motion and continuing after the lava surface came to rest. Competent layered material within the steep crater walls of VRC craters suggests that the rootless tephra was erupted in a partially molten state and that the spatter clasts fused together to form indurated deposits in the upper portions of the vent-proximal cone facies. Consequently, rootless eruptions must have occurred before the core of the Tartarus Colles lava flow reached its solidus temperature.

[74] *Hamilton et al.* [2010c] adapted a conductive heat transfer model [*Carslaw and Jaeger*, 1986] to quantify the effects of a thermal pulse propagating from an active lava flow into an ice-bearing substrate. For conditions on Mars these simulations considered a baseline scenario with an ambient temperature of 210 K and a lava temperature of

1617 K. This temperature represents an initial basaltic magma temperature of 1450 K plus 167 K to account for the heat generated by the latent heat of magma crystallization. To describe lava-substrate heat transfer processes in the western Tartarus Colles region, *Hamilton et al.* [2010c] applied their model over a range of lava flow thicknesses up to 75 m, with initial ground ice concentrations ranging up to 30% (see section 2.5). In addition to calculating the maximum depth of the 273 K isotherm (i.e., ice melting temperature), they estimated the maximum depth of ground ice melting that could be achieved before the core of the lava flow cooled to its solidus temperature. For basaltic flows they assumed a solidus temperature of 1273 K and considered this isotherm to be significant because at subsolidus temperatures the lava would no longer be able to generate analogs to MFCI explosions. Nevertheless, this threshold is not a hard boundary because as lava cools its viscosity increases and the available thermal energy decreases, which leads to a gradual decrease in potential MFCI efficiency. Additionally, the solidus temperature of the lava depends on composition, which is poorly constrained for the Tartarus Colles volcanic unit. In this study, we have reapplied the model of *Hamilton et al.* [2010c] with ±200 K offsets in the 1273 K temperature criterion. For ambient temperature conditions of 210 ± 30 K, the expected range of ground ice melting when the lava core solidifies expands from a baseline scenario of ~0.6 times the lava flow thickness to approximately 0.4–0.9. Similarly, the absolute maximum depth of ground ice melting varies from a baseline scenario of ~2.2 times the lava flow thickness to approximately 1.7–3.4. Thus expected isotherm depths within the baseline scenario of *Hamilton et al.* [2010c] appear to be accurate within a factor of approximately ±2. Ratios of ground ice melting depth when the lava core solidifies to the depth when the 273 K isotherm reaches its absolute maximum depth are less sensitive to these uncertainties because they scale together, which results in ratios ranging from 0.25 to 0.27. Consequently, the maximum depth of ground ice melting that could be achieved by the time the lava core solidified is approximately a quarter of the total melting that could be achieved once the 273 K isotherm reached its maximum depth. This result is important because it demonstrates that after "dynamic" rootless eruptions cease to be possible, continued ground ice melting could mobilize considerable volumes of ground ice, which in turn could generate thermokarst if the H_2O were removed from beneath the flow (Figure 10).

[75] According to the baseline scenario of *Hamilton et al.* [2010c], a 30 m thick basaltic lava flow could melt ground ice to a depth of ~19 m by the time the flow core cooled to 1273 K. For ground ice contents ranging from 0 to 30%, this condition could have been reached 4–10 years after the lava was initially emplaced. However, meltwater production could have continued for about another 120–290 years as the 273 K isotherm penetrated to a maximum depth of ~66 m. Given otherwise identical conditions, the core of a 60 m thick

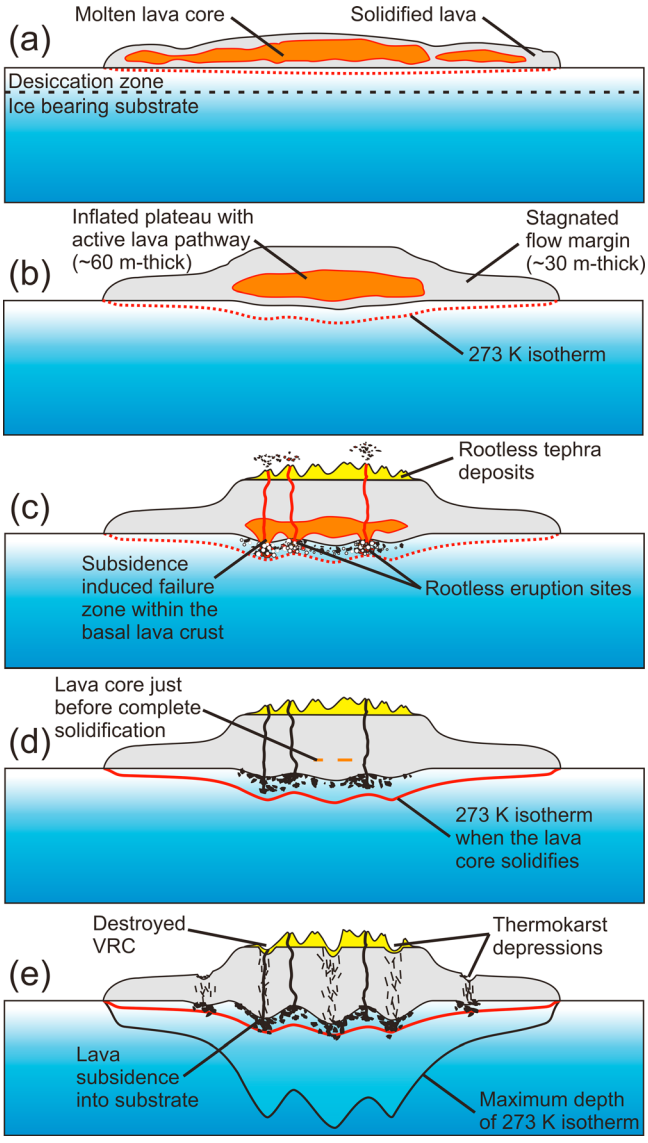

Figure 10. Conceptual model of lava–ground ice interactions in the western Tartarus Colles region viewed as a cross section through Tartarus Colles volcanic unit and underlying terrain with a lava flow direction into the page. Isotherm depths are drawn to scale with respect to the lava thickness, but the vertical scale is greatly exaggerated relative to the width. (a) The Tartarus Colles lava flow is emplaced above an ice-bearing substrate. (b) Concentrated flux of lava though central pathways enables these parts of the flow to inflate to ~60 m thickness, while the lateral flow margins stagnate at ~30 m thickness. (c) Heat is transferred from the lava to its surroundings, which melts ground ice as the substrate temperature reaches ~273 K. Ground ice melting allows the overlying lava to subside and founder into a deformable substrate. This brings molten lava and external water into direct contact and generates rootless eruptions. (d) The depth of the 273 K isotherm when the core of the lava solidifies constrains the ice table depth and maximum volume of meltwater that could have participated in the rootless eruptions. (e) Continued heat transfer from the lava to the substrate mobilizes additional H_2O, which gradually escapes to generate accommodation space beneath the lava. Collapse of the lava and overlying VRCs into the substrate generates pitted terrains throughout the Tartarus Colles volcanic unit and produces repelled distributions among surviving rootless eruption sites.

flow would have cooled to 1273 K after 10–50 years and attained melted ground ice to a depth of ~37 m. In contrast, maximum penetration of the 273 K isotherm would occur 340–1100 years later and achieve a depth of ~132 m. Thus, for 30–60 m thick lava flows, meltwater production could continue in the substrate for centuries after the last rootless constructs formed by MFCI mechanisms and, assuming an upper limit of 30% ice in the substrate, the lava could melt a maximum ice column thickness of 20–40 m (note that the column thickness refers to a hypothetical zone that ice would occupy if it were concentrated in a silicate-free layer [*Squyres et al.*, 1987]). The column thickness provides an upper limit to subsidence depths but should be regarded as overestimate because it assumes that all of the substrate contains 30% ice, all of the mobilized water escapes, and all of the vacated space could be completely compressed. Nonetheless, these results suggest that lava-induced thermokarstification could generate depressions that are of the order of meters to tens of meters, which is consistent with the observed depths of the pitted terrains in the Tartarus Colles volcanic unit. In this case, we attribute thermokarstification to melting of ice to differing depths within a permafrost that contains a homogeneous distribution of ground ice. However, heterogeneous concentrations of excess ice could also have an important role in generating collapse pits.

[76] On Earth, analogous thermokarst terrains have been described on the Seward Peninsula near Imuruk Lake in Arctic Alaska (65.6°N, 163.9°W). In this region the Lost Jim Lava Flow advanced >5 km over ice-rich permafrost [*Beget et al.*, 2007]. This basaltic lava flow includes unusually steep flow fronts and levees, with dips of up to 60° and heights of ~20 m. *Beget et al.* [2007] describe these flow margins as "super-inflated" structures and attribute their formation to enhanced cooling associated with steam that was produced by heating of the underlying ground ice by the active lava flow. The Lost Jim Lava Flow also includes complex thermokarst collapse features that were induced by melting of ground ice beneath the flow [*Beget et al.*, 2007; *Beget and Kargel*, 2008], thereby demonstrating that lava flows can melt significant volumes of ground ice in permafrost environments and that the withdrawal of water from the substrate can trigger the collapse of overlying lava.

[77] We have not observed any evidence of meltwater release onto the surface of the Tartarus Colles lava flow, or its surroundings, which suggests that after the last rootless eruptions occurred, additional H_2O was gradually lost from the substrate to the atmosphere through a permeable overburden and fractures in the overlying lava. An alternative hypothesis for the formation of the pitted terrains could involve ground ice removal by mechanisms that were unrelated to the emplacement of the Tartarus Colles lava flow (e.g., obliquity-driven climate change [*Laskar et al.*, 2004]), but given that pitted terrains are not observed in the surrounding Elyisum rise unit, such a hypothesis is unsupported.

6.2. Lava Surface Motion and its Geological Implications

[78] Evidence of widespread surface motion during the emplacement of the Tartarus Colles lava flow suggests that its emplacement was unlike typical 'a'a or pahoehoe flows. For instance, lava surface motion within 'a'a flows is dominantly confined to an active channel zone and the flow front, except where episodic overbank flows spill over the marginal channel levees [*Harris et al.*, 2009]. Relative to 'a'a flows, pahoehoe flows typically exhibit lateral crustal displacement over a much smaller proportion of their total area, with lateral surface motion generally confined to channels and the flow front [*Hon et al.*, 1994]. Where lava advances through the stochastic breakout of new toes from parent lobes [*Baloga and Glaze*, 2003]. The toes may develop into lobes and lava pathways (e.g., lava tubes) as the flow thickens through the endogeneous growth process of inflation [*Self et al.*, 1996, 1998]. Inflation involves vertical uplift of the lava surface, but generally occurs without significant horizontal displacement of the upper crust [*Hon et al.*, 1994]. Thus the Tartarus Colles lava flow does not fit well into the categories of either typical 'a'a or pahoehoe. Instead, it more closely resembles platy-ridged or rubbly pahoehoe lava surfaces [*Keszthelyi et al.*, 2000, 2004]. On Mars, similar lava flow surface textures occur in Tharsis, Amazonis Planitia, Elysium Planitia, Kasei Vallis, and Athabasca Valles [*Keszthelyi et al.*, 2000, 2004; *Jaeger et al.*, 2007, 2010]. These flows typically have margins that show evidence of inflation and surfaces composed of brecciated pahoehoe slabs and rubble plates ranging hundreds of meters to kilometers across [*Keszthelyi et al.*, 2000, 2004]. These plates can move in concert and effectively insulate the underlying core of the lava flow [*Keszthelyi et al.*, 2000, 2004]. This provides a mechanism by which tephra deposits erupted from multiple rootless eruption sites could have rafted downflow in unison to generate parallel arrangements of elongated VRCs in the Tartarus Colles region (e.g., Figures 3d–3f). Flow directions mapped by *Hamilton et al.* [2010c] suggest that the lava moved north through a narrow (~1.2 km wide) breach in the Nepenthes Mensae unit. Passage of lava through this constriction may have been responsible for disrupting the surface of the Tartarus Colles lava into rubble and large plates, in a process analogous to the formation of the platy-ridged surfaces on the Laki lava as it emerged from the confinement of the Skaftá river gorge and debouched onto the plains of southern Iceland [*Thordarson and Self*, 1993; *Keszthelyi et al.*, 2000, 2004; *Guilbaud et al.*, 2005]. Thus the discovery of platy-ridged lava flows in the Tartarus Colles region, in addition to Athabasca Valles and other volcanic regions on Mars [e.g., *Keszthelyi et al.*, 2000, 2004, 2008, 2010; *Jaeger et al.*, 2007, 2008, 2010], suggests that this style of lava emplacement is a recurring and important aspect of volcanic plains formation.

7. Conclusions

[79] Morphological and geospatial analyses of cratered cones and pitted terrains in the western Tartarus Colles region (25°N–27°N, 170°E–171°E) suggest that they are products of lava–ground ice interactions that involved both explosive and nonexplosive activity. Explosive lava-water interactions generated volcanic rootless constructs (VRCs) on the surface of the Tartarus Colles lava flow. Some rootless eruptions began while the platy-ridged surface was moving (thereby rafting rootless tephra deposits downflow to generate elongated VRC morphologies) whereas other rootless eruptions started after the flow surface came to rest, resulting in the construction of radially symmetric VRCs upon stationary surfaces. Within VRC domains that are defined by

convex hulls, rootless eruption sites appear to have generally formed independently of each other (i.e., randomly), but within the largest domains ($N \gtrsim 3000$) they exhibit statistically significant departures from randomness (beyond 2σ thresholds for R and c) with a tendency toward clustering. We interpret that this clustering is due to the preferential initiation of rootless eruptions within parts of the lava that were ~60 m thick because there was a critical lava thickness required for the lava to volatilize sufficient ground ice in the substrate before the core of the flow became too viscous to generate rootless explosions. Given that <0.3% of the rootless eruption sites occur where the lava is <30 m thick, we infer that, in general, this minimum lava thickness threshold was at least 30 m. After the main episodes of VRC formation, continued heat transfer melted additional ice in the substrate. Escape of mobilized H_2O then caused sections of the overlying lava to subside and founder into the substrate, generating pitted terrains throughout the Tartarus Colles lava flow. In the northern portions of the lava, where both VRCs and pitted terrains are most common, we infer that the observed tendency toward repelling in VRC-covered domains (i.e., regions defined by A rather than A_{hull}) was caused by thermokarstification, which generated greater than random NN distances between preserved rootless eruption sites by destroying some members of the initially random distributions.

[80] Evidence of complex VRC morphologies and emplacement chronologies within the western Tartarus Colles region demonstrate that the products of lava–ground ice interactions on Mars are not limited to isochronous groups of radially symmetric rootless cones and that variations in VRC characteristics can be used to infer information about lava emplacement dynamics and related geologic processes. This information is important for interpreting the paleoenvironmental significance of similar cone groups throughout Elysium Planitia and other regions of Mars. Additionally, if the VRCs and pitted terrains located throughout the broader Tartarus Colles region (25°N–28°N, 165°E–190°E [*Keszthelyi et al.*, 2010]) formed during the same volcanic episode, then an extensive fossil hydrothermal system may be located between northeastern Elysium Planitia and southern Arcadia Planitia. Given the potential magnitude of this volcanic event, the Tartarus Colles region could provide an ideal locality for investigating both volcanic plains formation and potential habitability of hydrothermal systems on Mars.

[81] **Acknowledgments.** We thank Pete Mouginis-Mark and the members of the MRO team for their assistance in acquiring the HiRISE targets used within this study. We are grateful to Scott Rowland, Bruce Houghton, Susanne Still, and Ciarán Beggan for their comments and suggestions during the preparation of this manuscript. We are also very appreciative of the thorough and insightful reviews provided by Laszlo Keszthelyi and Colin Dundas. Financial support was from NASA Mars Fundamental Research Program (MFRP) grant NNG05GM08G, NASA Mars Data Analysis Program (MDAP) grant NNG05GQ39G, and the Icelandic Center for Research (RANNÍS). This is SOEST publication 8056 and HIGP publication 1875.

References

Allen, C. C. (1979), Volcano-ice interactions on Mars, *J. Geophys. Res.*, *84*, 8048–8059.

Baloga, S. M., and L. S. Glaze (2003), Pahoehoe transport as a correlated random walk, *J. Geophys. Res.*, *108*(B1), 2031, doi:10.1029/2001JB001739.

Baloga, S. M., L. S. Glaze, and B. C. Bruno (2007), Nearest-neighbor analysis of small features on Mars: Applications to tumuli and rootless cones, *J. Geophys. Res.*, *112*, E03002, doi:10.1029/2005JE002652.

Beget, J. E., and J. Kargel (2008), Volcanoes and permafrost in Bering Land Bridge National Preserve, Arctic Alaska, pp. 32–37, Alaska Park Serv., U.S. Natl. Park Serv., Anchorage, Alaska.

Beget, J. E., J. Kargel, R. Wessels, and P. Layer (2007), Distinctive landforms produced by permafrost-volcano interactions, Arctic Alaska, paper presented at the 2nd Volcano-Ice Interaction of Earth and Mars Conference, Univ. of B. C., Vancouver, Canada.

Beggan, C., and C. W. Hamilton (2010), New image processing software for analyzing object size-frequency distribution, geometry, orientation, and spatial distribution, *Comput. Geosci.*, *36*, 539–549, doi:10.1016/j.cageo.2009.09.003.

Bishop, M. A. (2008), Higher-order neighbor analysis of the Tartarus Colles cone groups, Mars: The application of geographical indices to the understanding of cone pattern evolution, *Icarus*, *197*, 73–83.

Bruno, B. C., S. A. Fagents, T. Thordarson, S. M. Baloga, and E. Pilger (2004), Clustering within rootless cone groups on Iceland and Mars: Effect of nonrandom processes, *J. Geophys. Res.*, *109*, E07009, doi:10.1029/2004JE002273.

Bruno, B. C., S. A. Fagents, C. W. Hamilton, D. M. Burr, and S. M. Baloga (2006), Identification of volcanic rootless cones, ice mounds, and impact craters on Earth and Mars: Using spatial distribution as a remote sensing tool, *J. Geophys. Res.*, *111*, E06017, doi:10.1029/2005JE002510.

Burr, D. M., R. J. Soare, J.-M. Wan Bun Tseung, and J. P. Emery (2005), Young (late Amazonian), near surface, ground ice features near the equator, Athabasca Valles, Mars, *Icarus*, *178*, 56–73.

Burr, D. M., B. C. Bruno, P. D. Lanagan, L. S. Glaze, W. L. Jaeger, R. J. Soare, J.-M. Wan Bun Tseung, J. A. Skinner Jr., and S. M. Baloga (2009a), Mesoscale raised rim depressions (MRRDs) on Earth: A review of the characteristics, processes, and spatial distributions of analogs for Mars, *Planet. Space Sci.*, *57*, 579–596, doi:10.1016/j.pss.2008.11.011.

Burr, D. M., K. L. Tanaka, and K. Yoshikawa (2009b), Pingos on Earth and Mars, *Planet. Space Sci.*, *57*, 541–555, doi:10.1016/j.pss.2008.11.003.

Cabrol, N. A., E. A. Grin, and W. H. Pollard (2000), Possible frost mounds in an ancient Martian lake bed, *Icarus*, *145*, 91–107.

Carslaw, H. S., and J. C. Jaeger (1986), *Conduction of Heat in Solids*, 2nd ed., 510 pp., Oxford Univ. Press, New York.

Clark, P. J., and F. C. Evans (1954), Distance to nearest neighbor as a measure of spatial relationships in populations, *Ecology*, *35*, 445–453.

Clifford, S. M., and D. Hillel (1983), The stability of ground ice in the equatorial region of Mars, *J. Geophys. Res.*, *88*, 2456–2474.

Dundas, C. M., and A. S. McEwen (2010), An assessment of evidence for pingos on Mars using HiRISE, *Icarus*, *205*, 244–258.

Fagents, S. A., and T. Thordarson (2007), Rootless volcanic cones in Iceland and on Mars, in *The Geology of Mars: Evidence From Earth-Based Analogs*, edited by M. G. Chapman, pp. 151–177, Cambridge Univ. Press, Cambridge, U. K.

Fagents, S. A., P. Lanagan, and R. Greeley (2002), Rootless cones on Mars: A consequence of lava-ground ice interaction, in *Volcano-Ice Interaction on Earth and Mars*, edited by J. L. Smellie and M. G. Chapman, *Geol. Soc. Spec. Publ.*, *202*, 295–317.

Fanale, F. P., J. R. Salvail, A. P. Zent, and S. E. Postawko (1986), Global distribution and migration of subsurface ice on Mars, *Icarus*, *67*, 1–18.

Farrand, W. H., L. R. Gaddis, and L. Keszthelyi (2005), Pitted cones and domes on Mars: Observations in Acidalia Planitia and Cydonia Mensae using MOC, THEMIS, and TES data, *J. Geophys. Res.*, *110*, E05005, doi:10.1029/2004JE002297.

Fisher, R. V. (1968), Puu Hou littoral cones, Hawaii, *Geol. Rundsch.*, *57*, 837–864, doi.10.1007/BF01845368.

Fisher, R. V., and H.-U. Schmincke (1984), *Pyroclastic Rocks*, Springer, Berlin.

Frey, H., and M. Jarosewich (1982), Subkilometer Martian volcanoes: Properties and possible terrestrial analogs, *J. Geophys. Res.*, *87*, 9867–9879.

Frey, H., B. L. Lowry, and S. A. Chase (1979), Pseudocraters on Mars, *J. Geophys. Res.*, *84*, 8075–8086.

Frey, H., M. Jarosewich, and K. Partridge (1981), Pseudocraters near Hellas, *Lunar Planet. Sci. Conf.*, *22*, 300–302.

Fuller, E. R., and J. W. Head III (2002), Amazonis Planitia: The role of geologically recent volcanism and sedimentation in the formation of the smoothest plains on Mars, *J. Geophys. Res.*, *107*(E10), 5081, doi:10.1029/2002JE001842.

Graham, R. (1972) An efficient algorithm for determining the convex hull of a finite planar point set, *Inf. Proc. Lett.*, *1*, 132–133.

Greeley, R., and S. A. Fagents (2001) Icelandic pseudocraters as analogs to some volcanic cones on Mars, *J. Geophys. Res.*, *106*, 20,527–20,546.

Greeley, R., and P. D. Spudis (1981), Volcanism on Mars, *Rev. Geophys.*, *19*, 13–41.

Greeley, R., and E. Theilig (1978), Small volcanic constructs in the Chryse Planitia region of Mars, *Rep. TM-79729*, pp. 202–202, NASA Rep. Planet. Geol. Program.

Guilbaud, M.-N., S. Self, T. Thordarson, and S. Blake (2005), Flow formation, surface morphology, and emplacement mechanism of the AD 1783-4 Laki lava, in *Kinematics and Dynamics of Lava Flows*, edited by M. Manga and G. Ventura, *Spec. Pap. Geol. Soc. Am.*, *396*, 81–102.

Hamilton, C. W., and S. A. Fagents (2009), The Tartarus Colles cone group and its implications for explosive lava–water interactions in the Grjota Valles region of Mars, Abstract 1924 presented at the 40th Lunar and Planetary Sciences Conference (LPSC), Woodlands, Tex., 23–27 March.

Hamilton, C. W., T. Thordarson, and S. A. Fagents (2010a), Explosive lava-water interactions: I. Architecture and emplacement chronology of volcanic rootless cone groups in the 1783–1784 Laki lava flow, Iceland, *Bull. Volcanol.*, *72*, 449–467, doi:10.1007/s00445-009-0331-5.

Hamilton, C. W., S. A. Fagents, and T. Thordarson (2010b), Explosive lava-water interactions: II. Self-organization processes among volcanic rootless eruption sites in the 1783–1784 Laki lava flow, Iceland, *Bull. Volcanol.*, *72*, 469–485, doi:10.1007/s00445-009-0331-5.

Hamilton, C. W., S. A. Fagents, and L. Wilson (2010c), Explosive lava-water interactions in Elysium Planitia, Mars: Geologic and thermodynamic constraints on the formation of the Tartarus Colles cone groups, *J. Geophys. Res.*, *115*, E09006, doi:10.1029/2009JE003546.

Harris, A. J. L., M. Favalli, F. Mazzarini, and C. W. Hamilton (2009) Construction dynamics of a lava channel, *Bull. Volcanol.*, *71*, 459–474, doi:10.1007/s00445-008-0238-6.

Hartmann, W. K. (2007), Martian cratering 9: Toward resolution of the controversy about small craters, *Icarus*, *189*, 274–278.

Hartmann, W. K., and D. C. Berman (2000), Elysium Planitia lava flows: Crater count chronology and geological implications, *J. Geophys. Res.*, *105*, 15,011–15,025.

Head, J. W., and L. Wilson (2002), Mars: A review and synthesis of general environments and geological settings of magma/H_2O interactions, in *Volcano-Ice Interaction on Earth and Mars*, edited by J. L. Smellie and M. G. Chapman, *Geol. Soc. Spec. Publ.*, *202*, 27–57.

Head, J. W., L. Wilson, and K. L. Mitchell (2003), Generation of recent massive water floods at Cerberus Fossae, Mars by dike emplacement, cryospheric cracking, and confined aquifer groundwater release, *Geophys. Res. Lett.*, *30*(11), 1577, doi:10.1029/2003GL017135.

Hon, K., J. Kauahikaua, R. Denlinger, and R. MacKay (1994), Emplacement and inflation of pahehoe sheet flows: Observations and measurements of active lava flows on Kilauea Volcano, Hawaii, *Geol. Soc. Am. Bull.*, *106*, 351–370.

Jaeger, W. L., L. P. Keszthelyi, A. S. McEwen, C. M. Dundas, and P. S. Russell (2007), Athabasca Valles, Mars: A lava-draped channel system, *Science*, *317*, 1709–1711, doi:10.1126/science.1143315.

Jaeger, W. L., L. P. Keszthelyi, A. S. McEwen, C. M. Dundas, and P. S. Russell (2008), Response to comment on "Athabasca Valles, Mars: A lava-draped channel system," *Science*, *320*, 1588c, doi:10.1126/science.1155124.

Jaeger, W. L., et al. (2010), Emplacement of the youngest flood lava on Mars: A short, turbulent story, *Icarus*, *205*, 230–243, doi:10.1016j.icarus.2009.09.011.

Jakosky, B. M., and E. L. Shock (1998), The biological potential of Mars, the early Earth, and Europa, *J. Geophys. Res.*, *103*, 19,359–19,364.

Jerram, D. A., M. J. Cheadle, R. H. Hunter, and M. T. Elliot (1996), The spatial distribution of crystals in rocks, *Contrib. Mineral. Petrol.*, *125*, 60–74.

Jurado-Chichay, Z., S. K. Rowland, and G. P. L. Walker (1996), The formation of circular littoral cones from tube-fed pahoehoe: Mauna Loa, Hawaii, *Bull. Volcanol.*, *57*, 471–482, doi:10.1007/BF00304433.

Kauahikaua, J., D. R. Sherrod, K. V. Cashman, C. Heliker, K. Hon, T. N. Mattox, and J. A. Johnson (2003), Hawaiian lava-flow dynamics during the Pu'u 'O'o-Kupaianaha eruption: A tale of two decades, *U.S. Geol. Surv. Prof. Pap.*, *1676*, 63–87.

Keszthelyi, L., A. S. McEwen, and T. Thordarson (2000), Terrestrial analogs and thermal models for Martian flood lavas, *J. Geophys. Res.*, *105*, 15,027–15,049.

Keszthelyi, L., T. Thordarson, A. McEwen, H. Haack, M. Guilbaud, S. Self, and M. J. Rossi (2004), Icelandic analogs to Martian flood lavas, *Geochem. Geophys. Geosyst.*, *5*, Q11014, doi:10.1029/2004GC000758.

Keszthelyi, L., W. Jaeger, A. McEwen, L. Tornabene, R. A. Beyer, C. Dundas, and M. Milazzo (2008), High Resolution Imaging Science Experiment (HiRISE) images of volcanic terrains from the first 6 months of the Mars Reconnaissance Orbiter Primary Science Phase, *J. Geophys. Res.*, *113*, E04005, doi:10.1029/2007JE002968.

Keszthelyi, L., W. Jaeger, C. Dundas, S. Martínez-Alonso, A. S. McEwen, and M. P. Milazzo (2010), Hydrovolcanic features on Mars: Preliminary observations from the first Mars year of HiRISE imaging, *Icarus*, *205*, 211–229, doi:10.1016/j.icarus.2009.08.020.

Lanagan, P. D., A. S. McEwen, L. P. Keszthelyi, and T. Thordarson (2001), Rootless cones on Mars indicating the presence of shallow equatorial ground ice in recent times, *Geophys. Res. Lett.*, *28*, 2365–2367.

Lanz, J. K., and M. B. Saric (2009), Cone fields in SW Elysium Planitia: Hydrothermal venting on Mars?, *J. Geophys. Res.*, *114*, E02008, doi:10.1029/2008JE003209.

Laskar, J., A. C. M. Correia, M. Gastineau, F. Joutel, B. Levrard, and P. Robutel (2004), Long term evolution and chaotic diffusion of the insolation quantities of Mars, *Icarus*, *170*, 343–364.

Link, L. S., B. Jakosky, and G. D. Thyne (2005), Biological potential of low-temperature aqueous environments on Mars, *Int. J. Astrobiol.*, *4*, 155–164, doi:10.1017/S1473550405002648.

Lucchitta, B. K. (1978), Geologic map of the Ismenius Lacus Quadrangle, Mars, scale 1:5,000,000, *U.S. Geol. Surv. Misc. Invest. Map, I-1065*.

Lucchitta, B. K. (1981), Mars and Earth: Comparison of cold climate features, *Icarus*, *45*, 264–303.

Malin, M. C., G. E. Danielson, A. P. Ingersoll, H. Masursky, J. Veverka, M. A. Ravine, and T. A. Soulanille (1992), The Mars Observer Camera, *J. Geophys. Res.*, *97*, 7699–7718.

Mars Exploration Program Analysis Group (MEPAG) (2008), Mars scientific goals, objectives, investigations, and priorities, edited by J. Grant, 37 pp., white paper, Pasadena, Calif. (Available at http://mepag.jpl.nasa.gov/reports/index.html)

McGowan, E. (2009), Spatial distribution of putative water related features in Southern Acidalia/Cydonia Mensae, Mars, *Icarus*, *202*, 78–89, doi:10.1016/j.icarus.2009.02.024.

Mellon, M. T., and B. M. Jakosky (1995), The distribution and behavior of Martian ground ice during past and present epochs, *J. Geophys. Res.*, *100*, 11,781–11,799.

Mouginis-Mark, P. J. (1985), Volcano-ground ice interactions in Elysium Planitia, Mars, *Icarus*, *88*, 265–284.

Page, D. P. (2007), Recent low-latitude freeze-thaw on Mars, *Icarus*, *189*, 83–117.

Page, D. P. (2008), Comment on "Athabasca Valles, Mars: A lava-draped channel system," *Science*, *320*, 1588, doi:10.1126/science.1154849.

Page, D. P., and J. B. Murray (2006), Stratigraphical and morphological evidence for pingo genesis in the Cerberus plains, *Icarus*, *183*, 46–54.

Page, D. P., M. R. Balme, and M. M. Grady (2009), Dating Martian climate change, *Icarus*, *203*, 376–389.

Plescia, J. B. (2003), Cerberus Fossae, Elysium, Mars: A source for lava and water, *Icarus*, *164*, 79–95.

Rittman, A. (1938), Die Vulkan am Myvatn in Nord-Island, *Bull. Volcanol.*, *4*, 1–38.

Selby, M. J. (1993), *Hillslope Materials and Processes*, 451 pp., Oxford Univ. Press, Oxford, U. K.

Self, S., T. Thordarson, L. Keszthelyi, G. P. L. Walker, K. Hon, M. T. Murphy, P. Long, and S. Finnemore (1996), A new model for the emplacement of Columbia River Basalts as large, inflated pahoehoe lava flow fields, *Geophys. Res. Lett.*, *23*, 2689–2692.

Self, S., L. Keszthelyi, and T. Thordarson (1998), The importance of pahoehoe, *Ann. Rev. Earth Planet. Sci.*, *26*, 81–110.

Sheth, H. C., G. Mathew, K. Pande, S. Mallick, and B. Jena (2003), Cones and craters on Mount Pavagadh, Deccan Traps: Rootless cones?, *J. Earth Syst. Sci.*, *113*, 831–838, doi:10.1007/BF02704041.

Shock, E. L. (1997), High temperature life without photosynthesis as a model for Mars, *J. Geophys. Res.*, *102*, 23,687–23,694.

Squyres, S. W., D. E. Wilhelms, and A. C. Moosman (1987), Large-scale volcano-ground ice interactions on Mars, *Icarus*, *78*, 385–408.

Squyres, S. W., S. M. Clifford, R. O. Kuzmin, J. R. Zimbelman, and F. M. Costard (1992), Ice in the Martian regolith, in *Mars*, edited by H. H. Kieffer et al., pp. 523–554, Univ. of Ariz. Press, Tucson.

Sullivan, R., P. Thomas, J. Veverka, M. Malin, and K. S. Edgett (2001), Mass movement slope streaks imaged by the Mars Orbiter Camera, *J. Geophys. Res.*, *106*, 23,607–23,633.

Tanaka, K. L., J. A. Skinner, and T. M. Hare (2005), Geologic map of the northern plains of Mars, *U.S. Geol. Surv. Sci. Invest. Map*, *2888*.

Thorarinsson, S. (1951), Laxargljufur and Laxarhraun: A tephrochronological study, *Geogr. Ann.*, *H1-2*, 1–89.

Thorarinsson, S. (1953), The crater groups in Iceland, *Bull. Volcanol.*, *14*, 3–44.

Thordarson, T., and A. Höskuldson (2002), *Classic Geology in Europe 3: Iceland*, 200 pp., Terra Publ., Harpenden, U. K.

Thordarson, T., and S. Self (1993), The Laki (Skaftár Fires) and Grímsvötn eruptions in 1783–1785, *Bull. Volcanol.*, *55*, 233–263.

Thordarson, T., D. J. Miller, and G. Larsen (1998), New data on the Leidolfsfell cone group in South Iceland, *Jökull*, *46*, 3–15.

von Komorowicz, M. (1912), *Vulkanologische Studien auf Einigen Inseln des Atlantichen Oceans*, 189 pp., E. Schweizerbart, Stuttgart, Germany.
Wilson, L., and J. W. Head III (2007), Heat transfer in volcano-ice interactions on Earth, *Ann. Glaciol.*, *45*, 83–86.
Wohletz, K. H. (1986), Explosive magma-water interactions: Thermodynamics, explosion mechanisms, and field studies, *Bull. Volcanol.*, *48*, 245–264.
Wohletz, K. H. (2002), Water/magma interaction: Some theory and experiments on peperite formation, *J. Volcanol. Geotherm. Res.*, *114*, 19–35.

S. A. Fagents and C. W. Hamilton, Hawaii Institute of Geophysics and Planetology, University of Hawai'i, 1680 East-West Rd., Honolulu, HI 96822, USA. (christopher@higp.hawaii.edu)

T. Thordarson, School of Geosciences, University of Edinburgh, Grant Institute, The King's Buildings, West Mains Road, Edinburgh EH9 3JW, UK.